HAL
open science

Shifts in growth light optima among diatom species support their succession during the spring bloom in the Arctic

Dany Croteau, Thomas Lacour, Nicolas Schiffrine, Philippe-Israël Morin, Marie-Hélène Forget, Flavienne Bruyant, Joannie Ferland, Augustin Lafond, Douglas Campbell, Jean-Éric Tremblay, et al.

To cite this version:

Dany Croteau, Thomas Lacour, Nicolas Schiffrine, Philippe-Israël Morin, Marie-Hélène Forget, et al.. Shifts in growth light optima among diatom species support their succession during the spring bloom in the Arctic. Journal of Ecology, 2022, 10.1111/1365-2745.13874 . hal-03652127

HAL Id: hal-03652127

https://hal.science/hal-03652127v1

Submitted on 26 Apr 2022

HAL is a multi-disciplinary open access archive for the deposit and dissemination of scientific research documents, whether they are published or not. The documents may come from teaching and research institutions in France or abroad, or from public or private research centers.

L'archive ouverte pluridisciplinaire **HAL**, est destinée au dépôt et à la diffusion de documents scientifiques de niveau recherche, publiés ou non, émanant des établissements d'enseignement et de recherche français ou étrangers, des laboratoires publics ou privés.

Received: 6 September 2021 | Accepted: 1 March 2022

DOI: 10.1111/1365-2745.13874

Journal of Ecology | BRITISH ECOLOGICAL SOCIETY

RESEARCH ARTICLE

Shifts in growth light optima among diatom species support their succession during the spring bloom in the Arctic

Dany Croteau[1,2] | Thomas Lacour[2,3] | Nicolas Schiffrine[2,4] | Philippe-Israël Morin[2] | Marie-Hélène Forget[2] | Flavienne Bruyant[2] | Joannie Ferland[2,5] | Augustin Lafond[6] | Douglas A. Campbell[7] | Jean-Éric Tremblay[2] | Marcel Babin[2] | Johann Lavaud[2,8]

[1]Institut de Biologie Physico-Chimique, Laboratory of Chloroplast Biology and Light Sensing in Microalgae, UMR7141, Centre National de la Recherche Scientifique (CNRS), Sorbonne Université, Paris, France; [2]Takuvik International Research Laboratory, Université Laval (Canada) - CNRS (France), IRL3376, Pavillon Alexandre-Vachon, Québec, QC, Canada; [3]IFREMER Unité PHYTOX, Laboratoire PHYSALG, Nantes, France; [4]Institut des sciences de la mer de Rimouski (ISMER), Université du Québec à Rimouski, Rimouski, Québec, QC, Canada; [5]Ministère de l'Environnement et de la Lutte contre les changements climatiques (MELCC), Québec, QC, Canada; [6]Aix-Marseille University, Université de Toulon, CNRS, IRD, MIO, UM 110, Marseille, France; [7]Biology Department, Mount Allison University, Sackville, NB, Canada and [8]UMR6539 LEMAR-Laboratoire des Sciences de l'Environnement Marin, CNRS/Univ Brest/Ifremer/IRD, Institut Européen de la Mer, Institut Universitaire Européen de la Mer, Technopôle Brest-Iroise, rue Dumont d'Urville, Plouzané, France

Correspondence
Dany Croteau
Email: croteau@ibpc.fr

Funding information
Canada First Research Excellence Fund; Canada Foundation for Innovation; Canadian Network for Research and Innovation in Machining Technology, Natural Sciences and Engineering Research Council of Canada, Grant/Award Number: RGPIN-2017-04505

Handling Editor: Dan A Smale

Abstract

1. Diatoms of the Arctic Ocean annually experience extreme changes of light environment linked to photoperiodic cycles and seasonal variations of the snow and sea-ice cover extent and thickness which attenuate light penetration in the water column. Arctic diatom communities exploit this complex seasonal dynamic through a well-documented species succession during spring, beginning in sea-ice and culminating in massive phytoplankton blooms underneath sea-ice and in the marginal ice zone. The pattern of diatom taxa sequentially dominating this succession is relatively well conserved interannually, and taxonomic shifts seem to align with habitat transitions.
2. To understand whether differential photoadaptation strategies among diatom taxa explain these recurring succession sequences, we coupled laboratory experiments with field work in Baffin Bay at 67.5°N. Based on field data, we selected five diatom species typical of different ecological niches and measured their growth rates under light intensity ranges representative of their natural habitats. To characterize their photoacclimative responses, we sampled pigments and total particulate carbon, and conducted ^{14}C-uptake photosynthesis response curves and variable fluorescence measurements.
3. We documented a gradient in species respective light intensity for maximal growth suggesting divergent light response plasticity, which for the most part align with species sequential dominance. Other photophysiological parameters supported this ecophysiological framing, although contrasts were always clear only between succession endmembers, *Nitzschia frigida* and *Chaetoceros neogracilis*. To validate that these photoacclimative responses are representative of in situ dynamics, we compared them to the chlorophyll *a*-specific light-limited slope (α^*) and saturated rate of photosynthesis (P^*_M), monitored in Baffin Bay on

 © 2022 British Ecological Society

sea-ice and planktonic communities. This complementary approach confirmed that unusual responses in α^* and P^*_M as a function of light history intensity are similar between sentinel sympagic species *N. frigida* and natural ice-core communities. While no light-history-dependent trends were observed in planktonic communities, their α^* and P^*_M values were in the range of measurements from our monospecific cultures.

4. *Synthesis*. Our results suggest that Arctic diatoms species photoadaptation strategy is tuned to the light environment of the habitats in which they dominate and indeed drives the seasonal taxonomic succession.

KEYWORDS
Arctic Ocean, diatoms, ecophysiology, photoacclimation, photoadaptation, primary production, seasonal species succession, spring bloom

1 | INTRODUCTION

Recurring patterns in photosynthetic taxa succession along disturbance gradients reflect intricate interplays between transient environmental components and taxa-specific functional traits, for instance, related to resource utilization (light and nutrients) and resilience to mortality factors (grazing, viral infections, etc.; Sommer et al., 2012; Chang et al., 2019; Caracciolo et al., 2021). Over a spring-to-summer succession, from sympagic (sea-ice) to planktonic growth forms, Arctic diatoms collectively exploit a wide range of environmental conditions through an extensive habitat shift: from dimly lit sea-ice brines (<1 μmol photons m^{-2} s^{-1} and minimal photoperiod; Hancke et al., 2018) to intensely illuminated open waters (up to approximately 1000 μmol photons m^{-2} s^{-1} and 24 h daylight; Massicotte et al., 2020; Figure 1). Differentially evolved capacities to exploit their dynamic light environment (photoadaptation) may translate into a key functional trait driving Arctic diatom seasonal taxonomic succession. On the one hand, light supply limits growth in winter and early spring (Leu et al., 2015; Randelhoff et al., 2020). On the other hand, excessive irradiance, heterogeneously distributed beneath the irregular snow and sea-ice cover (Katlein et al., 2016), can shape communities by excluding certain shade-adapted species later in the season (Galindo et al., 2017; Mundy et al., 2011). Although Arctic microalgae community composition varies both locally and interannually, typical trends show sequentially dominating diatom assemblages with changing growth forms (pennate vs. centric), taxa and life traits (e.g. colonial or solitary), seemingly aligned with habitat transition, especially during spring (Booth et al., 2002; Lafond et al., 2019; Luostarinen et al., 2020; von Quillfeldt, 2000).

Although some minimal photosynthetic plankton growth can occur earlier under fully ice-covered water (Randelhoff et al., 2020), the onset of the Arctic productive season is usually associated with the accelerating growth of sympagic microalgae in sea-ice. Sea-ice diatom blooms typically occur under thin snow-cover, and their occurrence increases as warmer temperature drives restructuring of snow crystals to a more translucent organization (Hancke et al., 2018). These sympagic microalgae communities are dominated by raphid pennate diatoms, particularly the sentinel Arctic sea-ice species, *Nitzschia frigida* (Poulin et al., 2011). Overall, sympagic primary productivity is lower than plankton productivity, but is key to ecological integrity for certain regions and benthic habitats where ice-algae represent the main (if not the only) autotrophic biomass influx (Koch et al., 2020). As snow melts, light penetrates deeper into ice-covered water where it can trigger substantial phytoplankton blooms (Ardyna et al., 2020; Arrigo et al., 2012), that may continue in the marginal ice zone (≈50% of water is ice-covered; Perrette et al., 2011). Productivity peaks along these successive bloom events are dominated by different taxonomic assemblages (Lafond et al., 2019). While pennate genera like *Fragilariopsis* and *Ceratoneis* (ex *Cylindrotheca*) colonizing both sea-ice and water (dual-forms) embody an important fraction of under-ice blooms, centric growth forms, overwhelmingly represented by the *Chaetoceros* and *Thalassiosira* genera, overtake pennate taxa in marginal ice zone blooms (Balzano et al., 2017; Booth et al., 2002; Lafond et al., 2019; Luostarinen et al., 2020). As nutrients pools become depleted in the photic zone, particularly silicic acid for diatoms (Krause et al., 2019), and grazing pressure increases, diatom dominance recedes and other important phytoplankton groups, including flagellates and haptophytes, usually proliferate (Blais et al., 2017).

Over this spring-to-summer transition, Arctic diatoms collectively exploit daily photosynthetically available radiation (PAR) shifting over 4 orders of magnitude through a combination of species-specific photoacclimation plasticity and a succession of species with distinct properties (Figure 1). Photosynthetic organisms respond to light limitation, typical of early Arctic spring under thick snow-cover (Alou-Font et al., 2013; Galindo et al., 2017), by increasing chlorophyll (Chl) *a* content and other important light harvesting pigments, like Chl *c* and fucoxanthin in diatoms. In light-saturating conditions, the bottleneck for photosynthesis is usually the temperature-dependent rate at which the Calvin–Benson–Bassham (CBB; Young et al., 2015). However, the relationship between carbon fixation and growth rate is seldom linear in microalgae (Halsey et al., 2010,

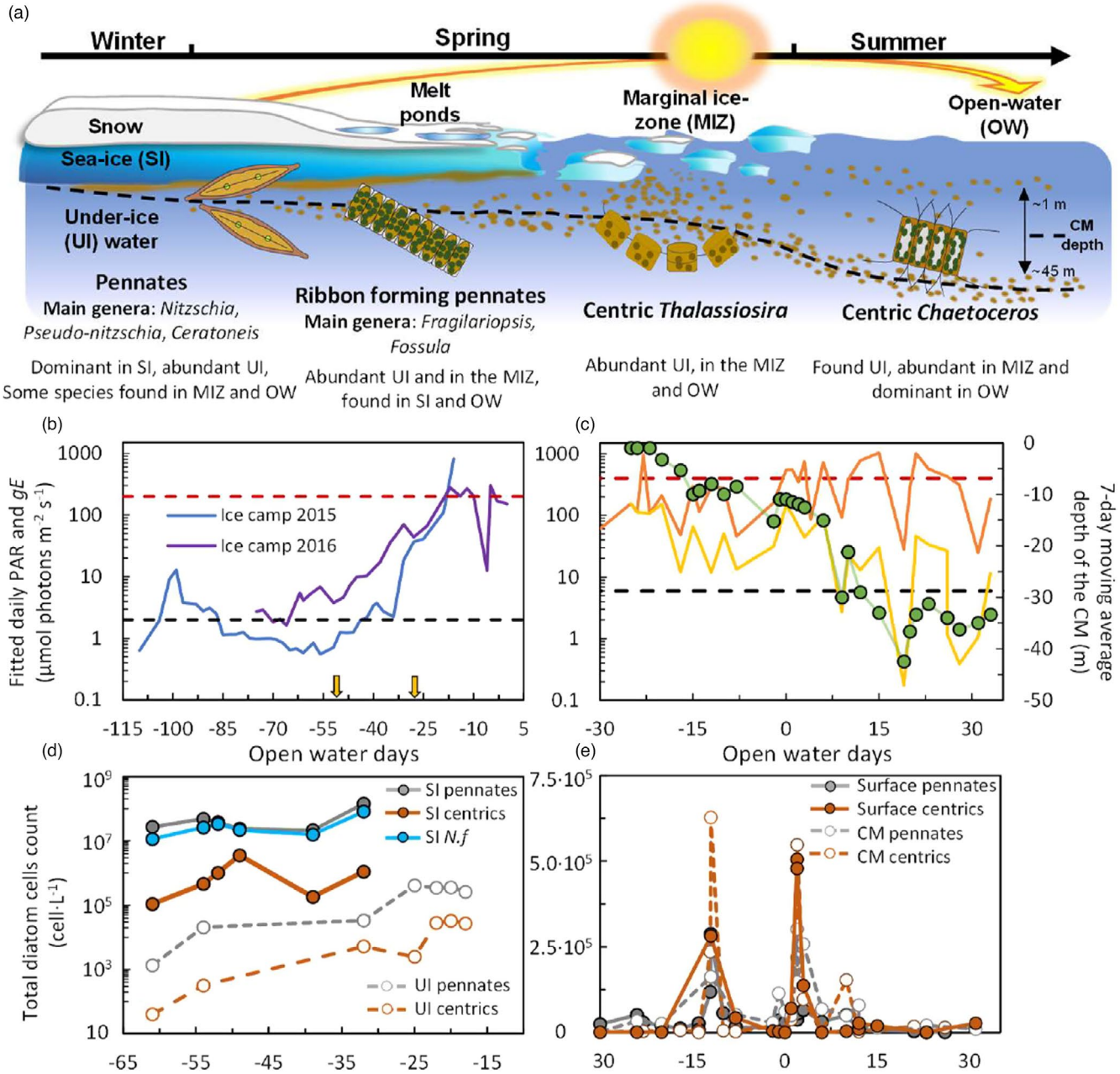

FIGURE 1 Schematic representation of a typical spring-to-summer Arctic diatom succession and the main observed diatom groups in Baffin Bay [where the Green Edge 2015–2016 ice-camps (67.48 N; 63.79 W) and 2016 oceanographic campaigns were conducted] over the habitat shift from snow-covered sea-ice to open waters (a) combined with physical and biological parameters assessed during the Green Edge project. Daily averaged photosynthetically available radiation (PAR) in µmol photons m^{-2} s^{-1} at the sea-ice-water interface during the 2015 and 2016 ice-camps (b), and at the water column surface (≈1 m) and at the chlorophyll *a* maximum (cm) and the 7-day moving average of the CM depth during the 2016 oceanographic campaign (c). PAR values are plotted versus open water days, where day 0 represents sea-ice breakup in (b and d) and the first three consecutive days of the season where roughly 50% of water is ice-covered in the transient marginal ice zone at a given sample station in (c and e). Horizontal dotted lines represent the minimal (black) or maximal (red) growth light (*gE*) used to grow either a sympagic (b) or a planktonic (c) diatom species during our laboratory study. In (b), yellow vertical arrows represent the average timing of snowmelt and melt ponds onset in that order. The repartition between pennates and centrics growth forms among diatom communities sampled in sea-ice (SI) and under-ice (UI) water from the 2016 ice-camp (d) and at surface level and at the CM on the oceanographic campaign (e) and the dominant sympagic species *N. frigida* (*N.f.*) which represented ≈60% of all cells counted in SI (d). See Material and Methods and Massicotte et al. (2020) for details on in situ measurements

2011), and has not been extensively studied in polar diatoms (Lacour et al., 2017). Under supersaturating light, as experienced by sympagic diatoms during the late spring melt period, photosynthesis can decrease due to photodamage and/or the induction of photoprotective mechanisms, such as the non-photochemical quenching (NPQ). Particularly crucial in diatoms, NPQ dissipates excess light energy as

harmless heat (Buck et al., 2019). Because NPQ in diatoms is mainly activated via the de-epoxidation of the xanthophyll pigment diadinoxanthin (DD) to diatoxanthin (DT), the magnitude of NPQ strongly depends on the cellular content of DD and DT (Lacour et al., 2020). Elevated NPQ results in a decrease in photosystem (PS) II quantum yield (F_V/F_M; parameters are defined in Figure S1) and effective absorption cross-section (σ_{PSII}; Buck et al., 2019), therefore impeding light energy transfer to photochemistry when NPQ is sustained as is common in polar strains (Lacour et al., 2018).

Arctic diatoms face unique photoadaptation challenges comprising scarce light availability for long periods over the annual cycle and a sluggish carboxylation rate of ribulose-1,5-bisphosphate (Rubisco) compromised by low temperatures (Young et al., 2015). Over generational-scale times, diatoms (and all photosynthetic organisms) can photoacclimate to a certain light regime, within a plasticity range anchored in genotypic photoadaptation defined over evolutionary times (Dubinsky & Stambler, 2009). Hence highlighting potentially contrasting photoadaption strategies, beyond the short-term photoacclimation state, entails studying growth light responses over a gradient rather than one or two light intensities. With this objective, we grew five ecologically relevant Arctic (or bipolar) diatom species under a range of limiting, saturating and supersaturating light typical of their respective habitats, and documented changes in their growth rates, photophysiology and carbon fixation capabilities. Most knowledge on Arctic diatom photoadaption at the moment is (i) inferred from correlation-based field observations (Kvernvik et al., 2021; Lewis et al., 2019; Schuback et al., 2017), (ii) assembled from independent studies targeting diverse photoadaptative traits in different polar species [reviewed by Lacour et al. (2017)] and/or (iii) extrapolated from laboratory studies in which most taxa occur only in Antarctic (Kulk et al., 2019; Petrou et al., 2011; Strzepek et al., 2019). However, we lack studies describing dose–response relationships between environmental factors and diverse species dominating distinct niches over seasonal dynamics required by production models and ecological theory.

Anthropogenic global warming may lead to a summer ice-free Arctic Ocean by the end of the century and therefore to exposure of Arctic microalgae to more light (Sigmond et al., 2018). Hence, a better description of Arctic diatom photoadaptation strategies across the wide ecodiversity spanning their productive season is imperative to better anticipate perturbations in succession dynamics, primary production and trophic transfers (Leu et al., 2016; Lewis et al., 2020). This paper is the second in a work series in which we investigate whether sequential taxa dominance of certain ecological niches over the Arctic seasonal light continuum is linked to interspecific photoadaptation divergences. Our previous report (Croteau et al., 2021) and Kvernvik et al. (2020, 2021) concluded that open-water Arctic diatom species are better equipped to cope with light stress than are sympagic species. To build upon these findings, we coupled field data from the Green Edge project 2015–2016 campaigns, which set out to unravel the seasonal dynamics steering Arctic microalgae spring blooms [see Green Edge Special Feature: Babin, 2019; Massicotte et al. (2020)], to the investigation of growth-light responses of five Arctic diatom species representing dominant groups from contrasting light environments over the spring-to-summer transition (Lafond et al., 2019; Figure 1). This refined resolution of Arctic diatoms light adaptation reveals that species-specific ascending growth light optima mostly align with their sequential seasonal dominance with profound low-light versus high-light specialization between sympagic and open-water succession endmembers. Moreover, photosynthetic parameters measured in laboratory with sentinel sympagic *Nitzschia frigida* reflected contrasts between sea-ice and planktonic natural communities and showed similar light intensity response as sea-ice samples, validating the value of our ecological niche resolved approach.

2 | MATERIALS AND METHODS

2.1 | Coupling of laboratory study to in situ data of Arctic diatom seasonal succession from the Green Edge database

The Green Edge project conducted two field campaigns (2015–2016) at an ice-camp located on landfast sea-ice (south from Qikiqtarjuaq Island in Baffin Bay), and one offshore oceanographic campaign over Baffin Bay onboard the *CCGS Amundsen* (2016) to study the processes steering Arctic ice-algae and phytoplankton spring blooms (Babin, 2019). The Nunavut government issued the Scientific Research Licence 01010 15N-M and 01001 16R-M for the 2015 and 2016 campaigns, respectively. The Greenland Government additionally issued the licence #18789, no. 2772992, for the 2016 oceanographic campaign. Ice-camp sampling took place every second to third day at a fixed location (67.48 N, 63.79 W) from 28 March to 14 July 2015, and from 27 April to 22 July 2016 (see Oziel et al., 2019). Sampling during the oceanographic campaign was achieved at 135 stations distributed over 7 zonal transects perpendicular to the ice edge, and each spanning about 120 miles over the ice-covered, marginal ice zone and open-water areas, which corresponded to early-bloom, bloom and post-bloom conditions, respectively. The array of bio-physicochemical parameters documented during the campaigns were gathered in a database available online (http://www.obs-vlfr.fr/proof/php/GREENEDGE/greenedge.php; see also Massicotte et al., 2020). We used Green Edge data to design our laboratory experiments to be representative of the Arctic Ocean seasonal dynamics with regards to growth light and selection of diatom species. We briefly described how Green Edge data were collected, summarizing key results regarding Arctic diatom succession and the light environment in Figure 1. We refer readers to the cited works for details on the methods, results and discussion.

During the Green Edge oceanographic campaign, measurements at a given date and sampling station were associated with a proxy of 'open water days' (OWD) to reconstruct seasonal phenology relative to sea-ice dynamics rather than location or calendar days (see Randelhoff et al., 2019). For every sampling station

during the oceanographic campaign, we assigned the number of days elapsed since the first occurrence of three consecutive days with ≤50% ice-cover at the station location. A negative OWD therefore indicates the number of days before sea-ice breakup. Thus, depending upon latitudinal variability in sea-ice melt progress, it is possible to find two samplings (from different stations) with a same OWD (see Figure S2 for the *CCGS Amundsen* itinerary, sampling stations and corresponding OWD). For ice-camp measurements, OWD = 0 is assigned to the date of sea-ice breakup. The photosynthetically available radiation (PAR) was obtained by monitoring downwelling irradiance above the surface and underwater over a vertical profile down to 100 m using a C-OPS underwater spectroradiometer (Compact Optical Profiling System; Hooker et al., 2013) and integrating irradiance from 400 to 700 nm. The 24 h PAR at a given depth was calculated by multiplying the surface level 24 h irradiance by the instantaneous transmittance given by the ratio between underwater irradiance and above the surface irradiance (Massicotte et al., 2020). To estimate the light exposure Arctic sympagic diatoms experience seasonally, we plotted the daily averaged PAR at sea-ice-water interface for a given day, in µmol photons m^{-2} s^{-1}, as a function of its associated OWD over the 2015–2016 ice-camp campaigns (Figure 1b; noteworthy, this method underestimates incident PAR on ice-algae since some light is absorbed by ice-algae). To estimate the light exposure Arctic planktonic diatoms experience, we plotted the daily averaged PAR for a given day at the surface (≈1 m) and at the depth of the Chl *a* maximum (CM) for the days of taxonomic sampling as a function of its associated OWD over the 2016 oceanographic campaign (Figure 1c).

Ice-core and water column samples were collected and analysed by inverted microscopy for identification and quantification (Utermöhl method). We regrouped diatom counts at the genus level for sea-ice communities, under-ice communities and open water planktonic communities (see Lafond et al., 2019) at the surface level and at the Chl *a* maximum (Figure S3). Parameters retrieved from ^{14}C-uptake photosynthesis response curves performed (as describe below) on ice cores and water column samples were used for comparison purposes with our laboratory-grown species (see Section 3).

2.2 | Acclimation of algal cultures

Unialgal cultures of *Nitzschia frigida* (A. Juhl), *Fragilariopsis cylindrus* (CCMP1102), *Thalassiosira gravida* (CCMP986), *Chaetoceros neogracilis* (RCC2278) and *Chaetoceros gelidus* (RCC2046; Table 1) were grown in filtered (0.2 µm) seawater (Baffin Bay, 67.48 N; 63.79 W) enriched in *f*/2 medium with silicate in a 0°C cold room, constantly illuminated under a 24 h photoperiod. CCMP1102 is the model *F. cylindrus* strain which was isolated from Antarctic and whose genome is sequenced (Mock et al., 2017), but this species is also abundantly reported in the Arctic (Luostarinen et al., 2020; Poulin et al., 2011). For the sake of space, we will refer to the five species studied together as 'Arctic species' from here onward. Culture triplicates were maintained in semi-continuous growth by diluting cultures with fresh medium every second day, and gently aerated with air passed through 0.3-µm-pore filters. Cultures were grown under a range of growth light intensities (*gE*, µmol photons m^{-2} s^{-1}) which were selected to cover light limitation, light saturation and supersaturating light conditions for every species (2–400 µmol photons m^{-2} s^{-1}). The growth lights were measured with a QSL-100 quantum sensor (Biospherical Instruments) placed in the culture vessel. Because of slow growth rates in Arctic diatoms, especially for sympagic species under low light, we proceeded to measurements after a maximum of 3 weeks of acclimation even if the typical 10 rounds of cellular division usually prescribed for

TABLE 1 Important diatom species in Arctic investigated in this study with their defining growth forms, life mode, habitats and the depth and coordinates at which the strains were isolated and their reference. Habitats are sea-ice (SI), under-ice water (UI), marginal ice zone (MIZ) and open water (OW), the round symbols referred to whether a species is rarely or not found (no symbol), commonly found •, abundant •• or dominant •••, in a given habitat. Color shading under column 1 references the color of the symbols associated to each species in all figures throughout the manuscript

Species	Growth form	Life mode	Habitats				Isolation		Strain reference
			SI	UI	MIZ	OW	Depth (m)	Coordinates	
***Nitzschia frigida* N.f.**	Pennate	Sympagic	•••	•	•		Sea-ice	NA[a]	A.R. Juhl
***Fragilariopsis cylindrus* F.c.**	Pennate	Dual form	•	••	••	•	Unknown	64.08°S 48.70°W[b]	CCMP1102
***Thalassiosira gravida* T.g.**	Centric	Planktonic		••	•••	••	30	69.67°N 18.97°W	CCMP986
***Chaetoceros neogracilis* C.n.**	Centric	Planktonic		•	••	••	3	71.57°N 133.95°W	RCC2278
***Chaetoceros gelidus* C.g.**	Centric	Planktonic		•	••	•••	30	70.88°N 130.53°W	RCC2046

[a]The *N. frigida* strain was isolated near Barrow, AK, USA (Aumack & Juhl, 2015).

[b]CCMP1102 is the model genome sequenced *F. cylindrus* strain, which was isolated in Antarctic, but the species is found at both poles.

balanced growth were not reached (Wood et al., 2005). We chose this approach because for the slowest growth rates [≈0.05 d^{-1} (*N. frigida* under 2 μmol photons m^{-2} s^{-1})] reaching 10 rounds of cellular division would be much longer (≈5 months) than the phenological changes in light availability observed under the sea-ice cover which can increase by one order of magnitude over a period of 3 weeks (Figure 1b). Growth rates (μ, in d^{-1}) were calculated as:

$$\mu = \frac{\ln N_2 - \ln N_1}{t_2 - t_1} \quad (1)$$

where N_x is cellular concentration (in cell per ml) for a given day. The following quadratic equation presented in Eilers and Peeters (1988) was used to fit the relationship between the measured growth rates (μ, d^{-1}) and growth light intensity (gE):

$$\mu = \frac{gE}{agE^2 + bgE + c}, \quad (2)$$

for which the maximal growth rate (μ_M, in d^{-1}), the light intensity for maximal growth rate ($gE_{opt,}$ in μmol photons m^{-2} s^{-1}) and the initial slope of light-limited growth rate [α_μ, in d^{-1} m^2 mol $photons^{-1}$ (after unit conversion)] equal:

$$\mu_M = \frac{1}{b + 2\sqrt{ac}}, \quad (3)$$

$$gE_{opt} = \sqrt{\frac{c}{a}}, \quad (4)$$

$$\alpha_\mu = \frac{1}{c}. \quad (5)$$

2.3 | Cell growth, biovolume and chlorophyll a monitoring

Cell numbers and equivalent spherical volume were measured using a Beckman Multisizer 4 Coulter Counter except for *N. frigida* which the long and narrow shape required microscopy counting (Utermöhl method) and sizing ('cylinder + 2 half spheres' formula). Every 2 day, Chl *a* [extracted in acetone 90:10, volume:volume and estimated with a 10 AU fluorometer (Turner Designs)], growth rate and cell biovolume were monitored to assure these parameters remained stable between generations.

2.4 | Carbon content

Three technical replicates and blank of *f*/2 medium of 10 ml were sampled for each culture replicate for total particulate organic carbon analyses. The samples and blanks were filtered onto glass fibre filters (GF/F Whatman®, 0.7 μm nominal porosity, 25 mm diameter) pre-combusted at 500°C for 12 h. The filters were kept dry, before elemental analysis with a CHN analyser (2400 Series II CHNS/O, Perkin Elmer).

2.5 | Pigment analysis

For pigment analysis, 10 ml of samples of acclimated cultures was collected and immediately filtered onto glass fibre filters (Whatman®, 0.7 μm nominal porosity, 25 mm diameter), flash-frozen in liquid nitrogen and stored at −80°C until analysis. Samples extracted in 100% methanol were mixed (70:30, v/v) with a buffer solution [tetrabutylammonium acetate (28 mM)] following a method adapted from Ras et al. (2008). Pigment contents were measured by high-performance liquid chromatography with a Zorbax Eclipse XDB-C8 3.5 μm column (Agilent Technologies). The de-epoxidation state (DES, in %), representing a proxy of photoprotection and NPQ induction (Olaizola et al., 1994), was calculated as:

$$DES = \frac{DT}{DD + DT} \times 100, \quad (6)$$

where xanthophyll pigment DD is diadinoxanthin and DT is diatoxanthin (in mol per 100 mol Chl *a*).

2.6 | Photosynthesis light response curves of ^{14}C-uptake

The relationship between the rate of C-fixation and irradiance was determined by measuring ^{14}C-uptake in cultures subsamples exposed to a range of light levels for 20 min (PE curves) as in Morin et al. (2020). The following equation was fitted to the data (Platt et al., 1980):

$$P = P_S\left(1 - e^{\frac{-\alpha E}{P_S}}\right)e^{\frac{-\beta E}{P_S}} + P_0, \quad (7)$$

where E is the irradiance applied to a subsample (in μmol photons m^{-2} s^{-1}), α is the light-limited slope of the PE curves [in mgC m^{-3} h^{-1} (μmol photons m^{-2} s^{-1})$^{-1}$], P_S is the maximum carbon fixation rate in the absence of photoinhibition (in mgC m^{-3} h^{-1}), β is the photoinhibition coefficient [in mgC m^{-3} h^{-1} (μmol photons m^{-2} s^{-1})$^{-1}$] and P_0 is the *y*-intercept of the curve (in mgC m^{-3} h^{-1}). The maximum light saturated carbon fixation rate (P_M, in mgC m^{-3} h^{-1}) was calculated as:

$$P_M = P_S\left(\frac{\alpha}{\alpha+\beta}\right)\left(\frac{\beta}{\alpha+\beta}\right)^{\frac{\beta}{\alpha}}. \quad (8)$$

We normalized α and P_M to Chl *a* (α^* and P_M^*), and P_M also to total particulate C (in mg L^{-1}), P_M^C (in d^{-1}) after unit harmonization. The photoacclimation parameter (E_K, in μmol photons m^{-2} s^{-1}) was obtained by dividing P_M by α. To compare photosynthetic output and growth rates, we extrapolated the C-specific 20 min ^{14}C-uptake under a given growth light intensity to a per day value (P_{gE}, in d^{-1}). We determined P_{gE} by replacing the variables of Equation 7 by the fitted parameters of a PE curve and the corresponding growth light (gE) intensity under

which the diatoms were acclimated, normalized to total particulate C-content (TPC) and multiplied by 24:

$$P_{gE} = \left[P_S\left(1 - e^{\frac{-\alpha gE}{P_S}}\right)e^{\frac{-\beta gE}{P_S}} + P_0\right] \times \frac{1}{\text{TPC}} \times 24. \quad (9)$$

Because some photosynthates can be respired during the 20 min incubation, P_{gE} is not an exact measurement of gross carbon production (Halsey et al., 2010, 2011). However, dividing the measured growth rate (net production) by P_{gE} obtained under the same gE can give a rough estimate of relative growth efficiency (η_g, dimensionless) variations as a function of growth light intensity among species:

$$\eta_g = \frac{\mu_{gE}}{P_{gE}}. \quad (10)$$

2.7 | Variable chlorophyll a fluorescence measurements

Variable fluorescence measurements were made using a Fluorescence Induction and Relaxation (FIRe) fluorometer (Satlantic) that applies a saturating, single turnover flash (STF, 100 µs) of blue light (455 nm, 60 nm bandwidth) to the culture sample. The FIRe generates a Chl *a* fluorescence induction curve (detected at 680 nm) that can be used to estimate apparent size of PSII antenna functional cross-section (σ_{PSII}, in Å^2 quanta^{-1}), and the minimal (F_0) and maximal (F_M) dark-acclimated fluorescence using the MATLAB FIReWORX algorithm (https://sourceforge.net/projects/fireworx/). The σ_{PSII}, F_0 and F_M were measured on triplicate culture subsamples previously acclimated to the different growth lights, following 20 min of dark acclimation. The maximum quantum yield of PSII in the dark (F_V/F_M) was calculated as:

$$F_V / F_M = \frac{F_M - F_0}{F_M}. \quad (11)$$

2.8 | Curve fitting and data analysis

Curve fitting with nonlinear models and analysis of variance (ANOVA) were done in the R software environment. For curve fitting, we used the NLS.MULTSTART package (Padfield et al., 2021). Complete fits statistics and information are found in Supporting Information. ANOVA followed by Tukey's HSD test was conducted to compare the α^* and P^*_M among species and field samples collected either in ice-cores during the 2016 Green Edge ice-camp or in the water column during the 2016 Amundsen expedition (Massicotte et al., 2020; Oziel et al., 2019; Randelhoff et al., 2019). We excluded parameter values from plankton sampled below the photic zone [0.415 mol photons m^{-2} d^{-1} (Randelhoff et al., 2019; also lower than any gE used in laboratory besides for sympagic *N. frigida*)], sea-ice with values of $\alpha^* < 0.001$ and $P^*_M < 0.1$, which could stem from severe nutrient limitations in sea-ice brines or osmotic shock during melt procedures (Campbell et al., 2019) and outliers outside the range of mean ± 2.5 SD. For non-significantly different groups of a same habitat (i.e. *N. frigida* and *F. cylindrus* versus sea-ice samples or *F. cylindrus*, *T. gravida*, *C. neogracilis* and *C. gelidus* vs. planktonic samples), we used a second ANOVA and Tukey's HSD test to compare species/samples split in subgroups defined by their light history (LH). We used the gE_{opt} determined in laboratory to set LH boundaries relative to Arctic diatoms seasonal succession in situ. Low LH, medium LH and high LH were assigned to daily average gE/PAR of <40, between 40 and 80 and >80 µmol photons m^{-2} s^{-1}, respectively. The boundaries between the three LH categories were approximately set to the gE_{opt} of *F. cylindrus* (40 µmol photons m^{-2} s^{-1}) versus *T. gravida*/*C. gelidus* (80 µmol photons m^{-2} s^{-1}).

3 | RESULTS

3.1 | Growth rate as a function of growth light intensity

Maximal growth rate (μ_M) was the slowest in obligatory sympagic *N. frigida* (0.15 d^{-1}) and the fastest in open-water planktonic, often surface layer dominant, *C. neogracilis* (0.66 d^{-1}; Figure 1c; Balzano et al., 2017). In between, for the dual sympagic-planktonic form *F. cylindrus*, the sea-ice-associated planktonic *T. gravida* and the open-water planktonic, often dominant at the deep Chl *a* maximum *C. gelidus* (Balzano et al., 2017), μ_M was similar around 0.3 d^{-1} (Figure 1c). The initial slope of light-limited growth rate (α_μ) was lower in *F. cylindrus* and in *C. gelidus* (≈0.02) than in *N. frigida*, *T. gravida* and *C. neogracilis* which showed α_μ between ≈0.04 and 0.06 (Figure 3c). Like for the μ_M, *N. frigida* and *C. neogracilis* had the minimal and maximal values for the light intensity for maximal growth (gE_{opt}), respectively (23 vs. 206 µmol photons m^{-2} s^{-1}; Figure 3c). The gE_{opt} was clearly lower in *F. cylindrus* (46 µmol photons m^{-2} s^{-1}) than in *T. gravida* and *C. gelidus* (≈80 µmol photons m^{-2} s^{-1}; Figure 3c). The ninefold variation in gE_{opt} across species highlights different capacities in converting light to growth and contrasting photoadaption. Therefore, in the following sections, we will often refer to the dimensionless ratio of gE normalized to species-specific gE_{opt} to compare photoacclimation relative to growth potential across species (figures with gE rather than gE/gE_{opt} *x*-axis are found in Supporting Information).

3.2 | Carbon-to-chlorophyll a ratios

Among all species, the measured C-to-Chl *a* ratio ranged between 12 and 300 g·g^{-1} and was generally described by a linear increase as a function of gE intensity as proposed in Geider's model (1987; Figure 3). However, the minimal C-to-Chl *a* ratio was reached before

lowest *gE* intensity and stabilized, or was even higher, under the most limiting *gE*, except in *T. gravida*. We thus had to remove these points [and the lower ones in *N. frigida* grown under extreme supersaturating light (200 μmol photos m^{-2} s^{-1})] to compare the C-to-Chl *a* slope versus *gE* between species and with existing literature (Geider, 1987; Lacour et al., 2017). The steepest C-to-Chl *a* versus *gE* slopes were observed in *N. frigida* and *F. cylindrus*, and the lowest for *T. gravida* and *C. neogracilis*, with *C. gelidus* in between these extremes (Table 2). However, when C-to-Chl *a* was plotted against *gE* normalized to light intensity for maximal growth (gE/gE_{opt}; Figure 3b), both *Chaetoceros* species showed similar steeper slopes (≈43) after *F. cylindrus* (57; Table 2).

3.3 | Photosynthetic ^{14}C-uptake response curves parameters normalized to Chl a

Contrary to most previous results on temperate microalgae (MacIntyre et al., 2002) and some Arctic diatoms (see Sakshaug et al. (1991) and Section 4 below), the Chl *a*-specific light-limited slope of photosynthesis (α^*; Figure 4a) was strongly affected by *gE* intensity in all species, especially under light limitation and supersaturation. All species reached their highest α^* under the lowest *gE*, except for *F. cylindrus* for which a maximal plateau was maintained at average *gE* intensities (gE/gE_{opt} around ≈0.5; Figure 4a). At all *gE* intensities above the one corresponding to species respective maximal α^*, α^* was markedly lower although the decrease was steeper in *F. cylindrus*. Moreover, the Chl *a*-specific saturated rate of photosynthesis (P^*_M) as a function of gE/gE_{opt} (Figure 4b) was not systematically larger under higher gE/gE_{opt} as expected when investment in Chl *a* is reduced (Macintyre et al., 2002). Instead, contrasting patterns of P^*_M versus gE/gE_{opt} were observed across species, remaining roughly stable in *N. frigida*, being clearly lower for $gE/gE_{opt} > 1$ in *F. cylindrus* or steadily increasing in *T. gravida* and increasing even more in *C. neogracilis* (Figure 4b). Aside from the points at the lowest *gE* intensity in *F. cylindrus*, the photoacclimation parameter (E_K) followed a linear increase as a function of gE/gE_{opt}, with a steeper slope in *C. neogracilis* (72) and *T. gravida* (45) than in *N. frigida* and *F. cylindrus* (≈13; Figure S6).

TABLE 2 Slope and *y*-intercept (y_0) of the linear relationship between carbon to chlorophyll *a* (C-to-Chl *a*) ratio and growth light (*gE*) intensity and the dimensionless ratio between *gE* and *gE* for maximal growth rate (gE/gE_{opt}; y_0 and R^2 are independent of *x*-axis normalization). The values associated with open symbols in Figure 3a are excluded from the fits (see Sections 2 and 4)

	gE	gE/gE_{opt}		
Species	**Slope**	**Slope**	y_0	R^2
Nitzschia frigida	1.06	23.42	16.68	0.99
Fragilariopsis cylindrus	1.25	57.24	10.94	0.98
Thalassiosira gravida	0.16	13.00	23.57	0.89
Chaetoceros neogracilis	0.22	44.45	29.56	0.95
Chaetoceros gelidus	0.58	42.09	3.64	0.99

3.4 | Photosynthetic ^{14}C-uptake response curves parameters normalized to C and growth efficiency

In contrast to a previous review of temperate diatoms (MacIntyre et al., 2002), the C-specific light saturated rate of photosynthesis (P^C_M) responded strongly to *gE* in a similar pattern across species, albeit with varying amplitudes, the narrower in *C. neogracilis* and the wider in *F. cylindrus* (Figure 5a). We measured the maximal P^C_M in *Fragilariopsis cylindrus* under $gE/gE_{opt} \approx 1$, and under $gE/gE_{opt} < 0.4$ for the other species. Meaning that P^C_M were lower under more intense gE/gE_{opt} for all species, but also under lower gE/gE_{opt} when available (Figure 5a). In all species, the C-specific 20 min ^{14}C-uptake at a given *gE* extrapolated over 24 h (P_{gE}; Figure 5b) varied similarly to P^C_M. Growth rates were poorly predicted by P_{gE} changes within a species independent of light intensity, but rather seem to be distinctive characteristics among species, with *C. neogracilis* standing out with higher growth rates than all other species even at equal P_{gE} (Figure 5c). Variations in growth efficiency (η_g, Equation 10) as a function of gE/gE_{opt} showed a pattern inverse to those of P^C_M, reaching $\eta_g \approx 1$ under gE/gE_{opt} where P^C_M was at its lowest (Figure 5d). Except for *C. neogracilis*, which showed fairly consistent η_g between 0.8 and 1 across *gE*, all species showed large changes in η_g with minimal values between 0.3 and 0.5 (Figure 5d). Surprisingly, at the extremes of the *gE* intensities range *N. frigida* showed some η_g values above 1 (Figure 5d), which suggest the cells could not fully acclimate to these light intensities in 3 weeks and were possibly partly relying on carbon reserves or that some cells were dying due to light stress (see Section 4).

3.5 | Fluorometric index of photosystem II and xanthophyll pigments

The dark-acclimated quantum yield of PSII (F_V/F_M) was relatively stable within species under $gE < gE_{opt}$, but varied among species from ≈0.50 in *F. cylindrus* and *C. gelidus*, to ≈0.60 in *C. neogracilis* (Figure 6a). At $gE > gE_{opt}$, F_V/F_M sharply dropped by more than 50% in all species except *C. neogracilis*. Similar trends were observed for the effective absorption cross-section size of the antenna serving PSII (σ_{PSII}), ranging across species from 280 to 400 Å^2 quanta^{-1} under low-to-moderate growth light, and showing a ≈ 50% decrease under supersaturating light (Figure 6b). The lower values of F_V/F_M and σ_{PSII} paralleled a more than 10-fold increase in total xanthophyll pigments (diadinoxanthin and diatoxanthin) between the lowest and highest growth light intensity, across all species (Figure 6c). The de-epoxidation state, reflecting activated photoprotection via diadinoxanthin conversion to diatoxanthin, was also higher in all species

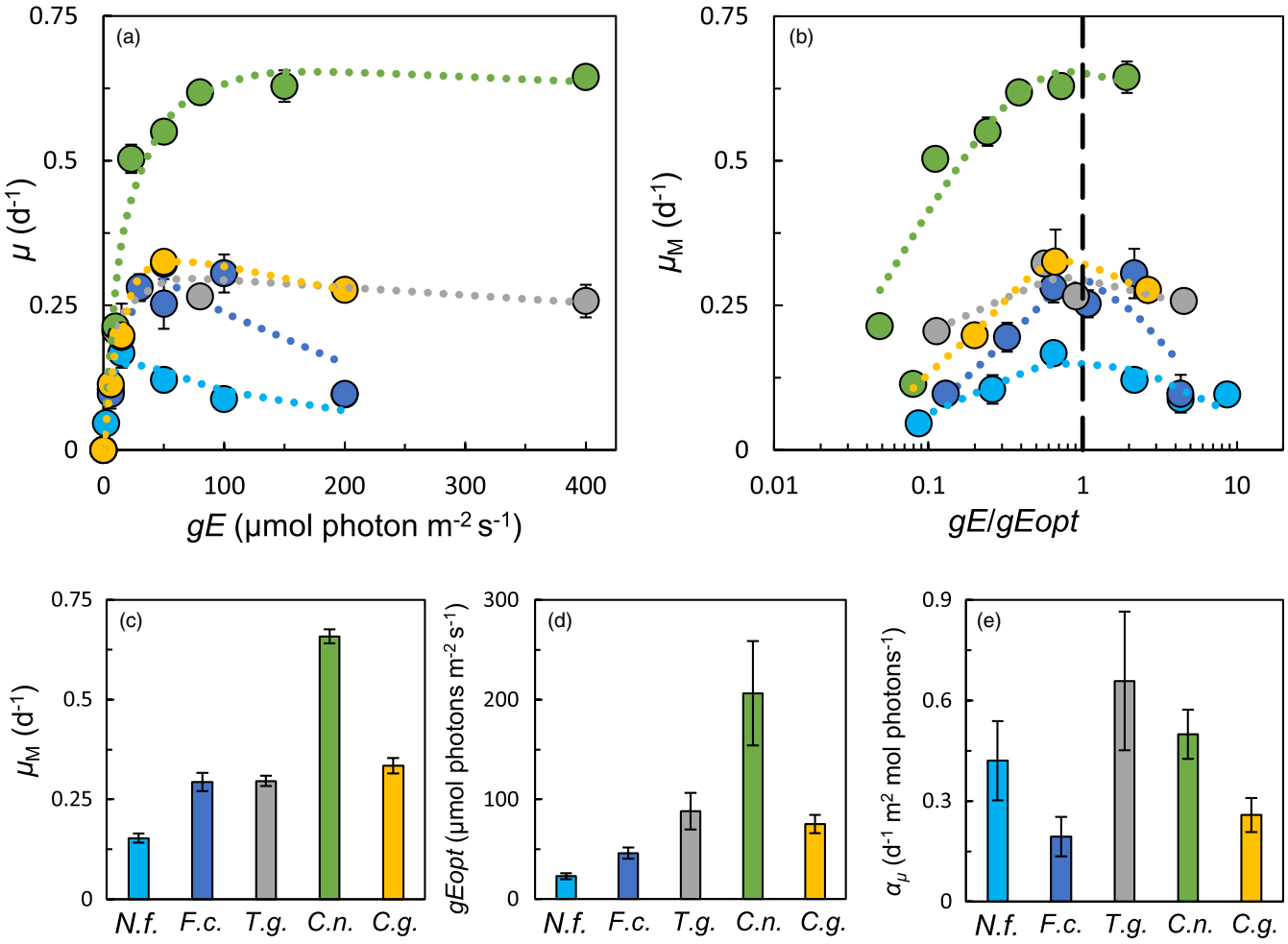

FIGURE 2 The measured growth rates (μ) plotted against growth light (gE) intensity (a) and the dimensionless ratio between gE and the gE for maximal growth rate (gE_{opt}), where the vertical dashed line represents $gE/gE_{opt} = 1$ (b), the maximal fitted μ (μ_M) (c), gE_{opt} (d) and the slope of light-limited μ (α_μ) (e) ± *SE* derived from the μ versus gE fitted curves in the five Arctic diatom species studied (see fit parameters in Supporting Information S4). Data points in (a) and (b) are triplicate mean ± SD. Species abbreviations are found in Table 1

under higher growth light intensities, but remained 2 to 3 times lower in *C. neogracilis* compared to the other species, even for similar gE/gE_{opt} (above 3; Figure 6d).

3.6 | ^{14}C-uptake response curves comparison between field samples and monospecific cultures

We used the ^{14}C-uptake response curves data measured in situ on sea-ice and planktonic communities during the Green Edge project (Massicotte et al., 2020; Oziel et al., 2019; Randelhoff et al., 2019) to compare to our laboratory measurements on monospecific cultures. Planktonic communities showed significantly higher ($p < 0.001$, all test results in Figure S11–S12) α^* (≈0.4 vs. 0.015) and P^*_M (≈1.4 vs. 0.5) compared to sea-ice communities (Figure 7a,b). The effect between low and high light history (LH) was significant only for α^* ($p < 0.01$) and we did not observe significant interaction between the two factors. Sentinel sympagic *N. frigida* was the only species which showed significantly different α^* and P^*_M values compared to planktonic communities but not with sea-ice ones. The other species that can grow in sea-ice, *F. cylindrus* was significantly different to sea-ice communities in both parameters. We further tested *N. frigida* and sea-ice samples responses in α^* and P^*_M depending upon LH by regrouping their respective parameters values in subgroups for the three different LH (Figure 7c,d). Overall, the trends with regards to LH intensity were similar, with the only significant being higher α^* for *N. frigida* than for natural sympagic communities under low LH ($p < 0.001$). Moreover, sea-ice samples showed a significant decreased in P^*_M between low and high LH, while *N. frigida* did not. There was no significant difference for both α^* ($p = 0.56$) and P^*_M ($p = 0.86$) when we compared the four species that can be abundant in the water column to natural planktonic samples (Figure S12).

4 | DISCUSSION

We set out to decipher the photoadaptation strategies of five diatom species important in the Arctic Ocean. We grew these species

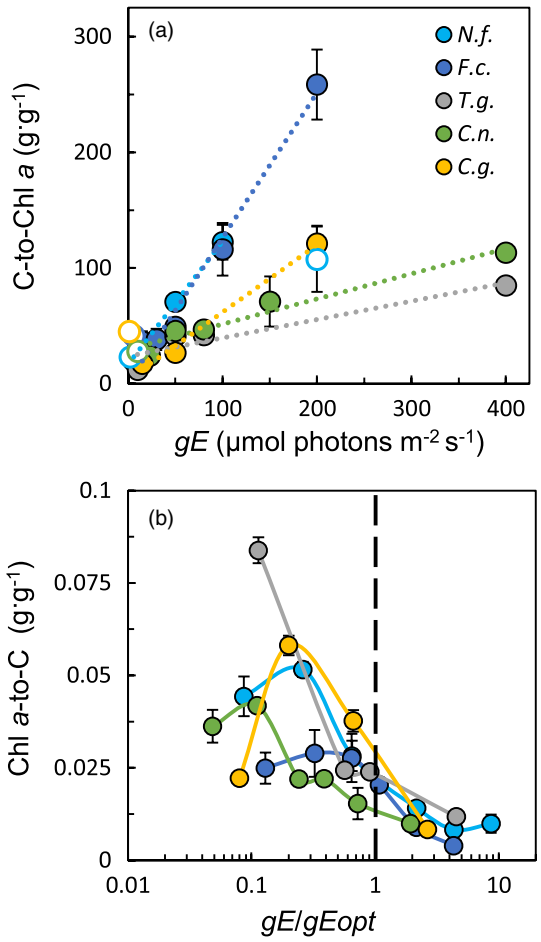

FIGURE 3 The linear regression between the C-to-chlorophyll *a* (C-to-Chl *a*) ratio and growth light (*gE*) intensity (a) and Chl *a*-to-C as a function of the dimensionless ratio between *gE* and *gE* for maximal growth rate (gE/gE_{opt}), where the vertical dashed line represents $gE/gE_{opt} = 1$ (b). Open symbols are excluded from the fits (see Sections 2 and 4). See linear equations parameters for C-to-Chl *a* as a function of *gE* and gE/gE_{opt} in Table 2. Data points are triplicate mean ± SD. Species abbreviations are found in Table 1

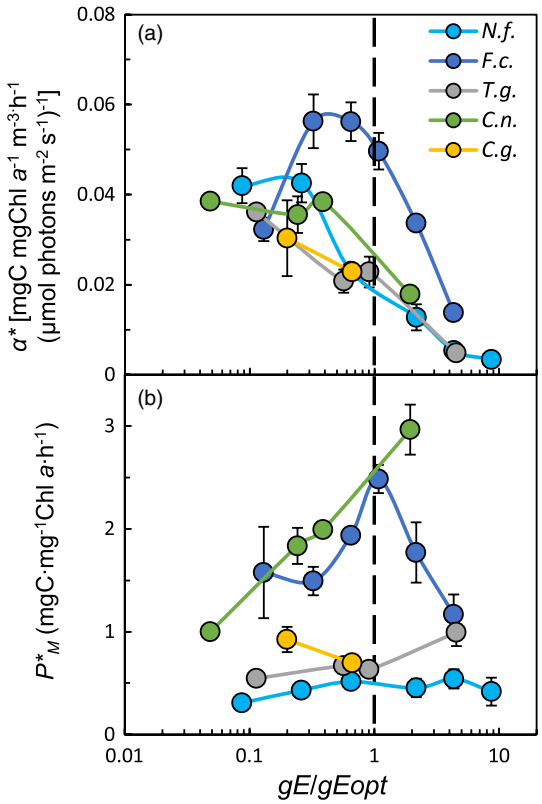

FIGURE 4 The chlorophyll (Chl) *a* specific light-limited slope of photosynthesis (α^*) (a) and light saturated rate of photosynthesis (P^*_M) (b) measured with ^{14}C-uptake photosynthesis response curves plotted versus the dimensionless ratio between growth light (*gE*) intensity and *gE* for maximal growth rate (gE/gE_{opt}), where the vertical dashed line represents $gE/gE_{opt} = 1$, in the five Arctic diatom species studied. All data points are triplicate mean ± SD. Species abbreviations are found in Table 1

over a wide range of ecologically representative growth light intensities (*gE*), to determine their photophysiological plasticity boundaries and relate these properties to the light niches where they are dominant/abundant over seasonal succession (Table 1). We documented a gradient in the species respective light intensities for maximal growth (gE_{opt}) suggesting divergent light response plasticity, for the most part aligning with species sequential dominance (Figure 2 and see species ecological niches in Figure 1 and Table 1). Other photophysiological parameters including productivity/growth rates, the early onset of DES increase relative to gE/gE_{opt} and sensitivity to photoinhibition, supported this ecophysiological framing, although some parameters only showed clear contrasts between the succession endmembers, *N. frigida* and *C. neogracilis*. For instance, dual sympagic-planktonic *F. cylindrus*, marginal ice zone dominant *T. gravida* and open-water *C. gelidus* showed similar μ_M of ≈ 0.3 d^{-1}, but only *F. cylindrus* suffered serious photoinhibition and growth rate decrease under $gE > gE_{opt}$ (Figure 2). Based on *N. frigida* and *C. neogracilis* photoadaptative strategies as well as field results on natural communities, we synthesized low-light/sympagic and high-light/open-water specialists' typical responses to light increase and linked it to in situ seasonal species succession and accompanying environment shifts (Figure 8).

4.1 | Extremes of the growth light gradient reveal atypical photoacclimative responses in Arctic diatoms

Acclimation patterns in many key photoacclimative features [C-to-Chl *a* ratio, the Chl *a*-specific initial slope of photosynthesis (α^*) and C-specific saturated rate of photosynthesis (P^C_M)] in the Arctic diatoms species studied were similar to expectations from temperate diatoms only over a narrow range of moderate growth light intensities (MacIntyre et al., 2002) while showing unexpected variations under light limitation ($gE << gE_{opt}$) or supersaturation ($gE > gE_{opt}$). It is important to investigate the nature of these findings as C-content and photosynthesis activity normalized to Chl *a* are keystone parameters of the photoacclimation model (Geider et al., 1998) on which

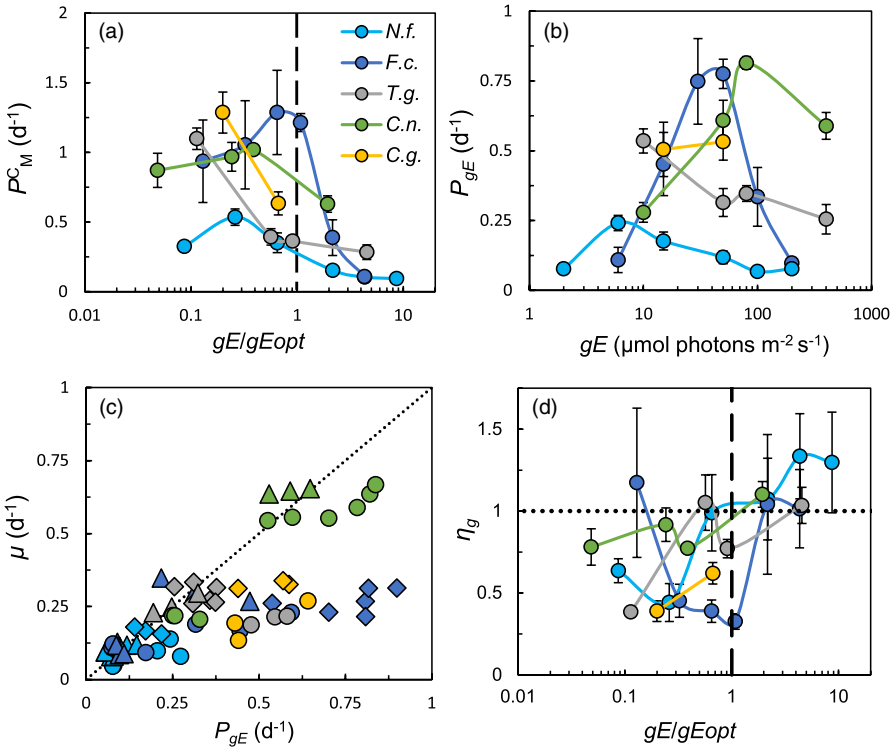

FIGURE 5 The carbon-specific maximal rate of photosynthesis (P^C_M) measured with ^{14}C-uptake photosynthesis response curves plotted versus the dimensionless ratio between growth light intensity (*gE*) and *gE* for maximal growth rate (gE/gE_{opt}) (a) and the C-specific 20 min ^{14}C-uptake under a given growth light (*gE*) intensity extrapolated over 24 hr (P_{gE}) plotted versus *gE* intensity (b). All growth rates (μ) measured across species plotted versus P_{gE} (c) and the growth efficiency (η_g) plotted versus gE/gE_{opt} (d). In a and c, the vertical dashed line represents $gE/gE_{opt} = 1$. In c, circles correspond to gE/gE_{opt} values <0.5, diamonds to values between 0.5 and 1, and triangles to values >1. The dotted line represents either the theoretical maximal 1:1 ratio between μ and P_{gE} in c, or a η_g of 1 in d. Except in c, all data points are triplicate mean ± SD. Species abbreviations are found in Table 1

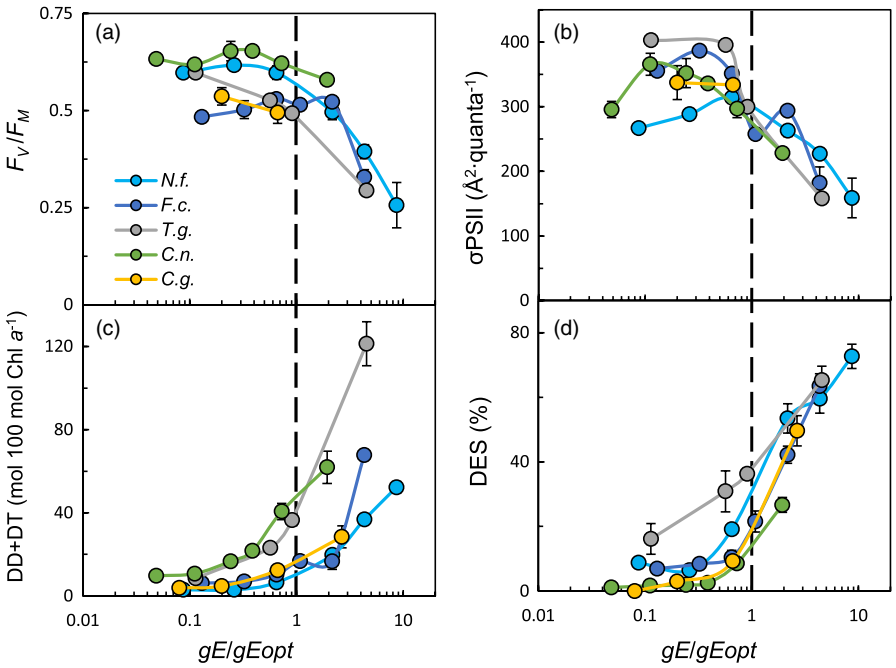

FIGURE 6 The dark-acclimated quantum yield of photosystem (PS) II (F_V/F_M) (a), the apparent size of PSII antenna functional cross-section (σ_{PSII}) (b), the sum of xanthophyll pigments diadinoxanthin (DD) and diatoxanthin (DT) (c) and the de-epoxidation state (DES) of the xanthophyll pool (d) plotted versus the dimensionless ratio between growth light (*gE*) intensity and *gE* for maximal growth rate (gE/gE_{opt}), where the vertical dashed line represents $gE/gE_{opt} = 1$, in the five Arctic diatom species studies. All data points are triplicate mean ± SD. Species abbreviations are found in Table 1. Fucoxanthin, chlorophyll *c* and β-carotene content are shown in Figure S10

several primary production (Bouman et al., 2018; Losa et al., 2019) and cell division rate (Randelhoff et al., 2020; Sathyendranath et al., 2009) models are based.

The C-to-Chl *a* parameter typically increases linearly with growth light intensity as cells decrease their investments in Chl *a* and light-harvesting proteins under more abundant light resource and is often

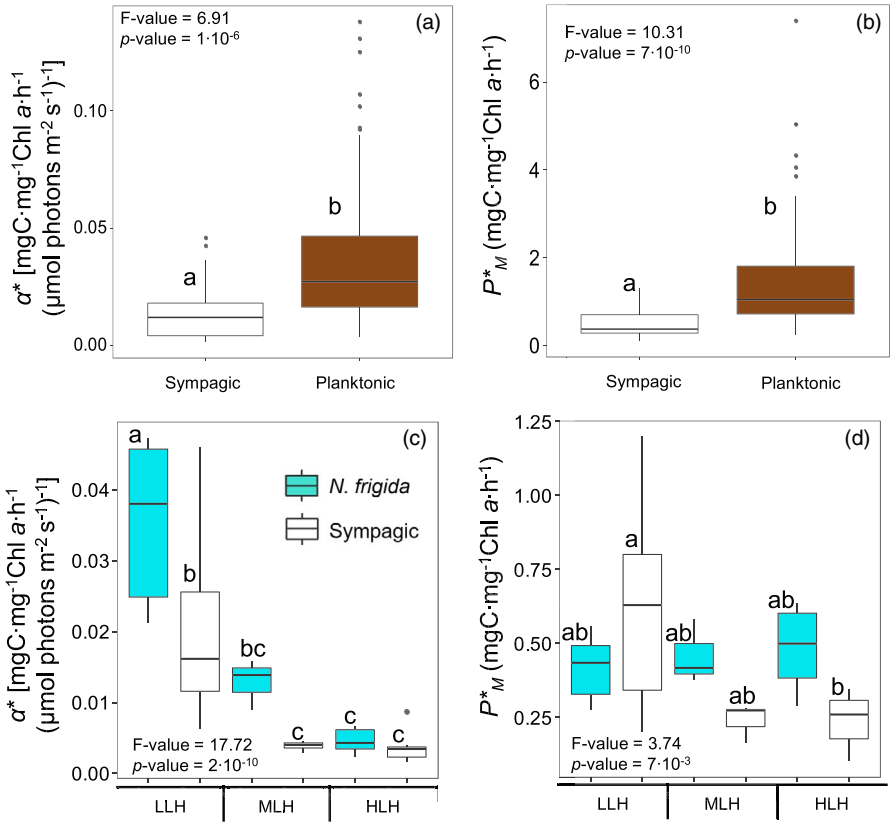

FIGURE 7 Boxplots comparing data distribution of chlorophyll (Chl) *a* specific light-limited slope of photosynthesis (α^*) (a) and light saturated rate of photosynthesis (P^*_M) (b) measured on sympagic communities sampled during the Green-Edge 2016 ice-camp and planktonic sampled communities during the 2016 Amundsen expedition. In (c) and (d), α^* and P^*_M are compared between laboratory monocultures of sentinel Arctic sympagic species *Nitzschia frigida* and sympagic communities, sub-grouped by light history (LH), that is, by growth light intensity (*gE*) for laboratory cultures or in situ photosynthetically available radiation (PAR) for natural communities. Low LH (LLH), medium LH (MLH) and high LH (HLH) are assigned to daily average *gE* or PAR of <40, between 40 and 80 and >80 µmol photons m^{-2} s^{-1}, respectively. ANOVA *F*-values and *p*-values are shown in each panel and different letters indicate significantly different groups by Tukey's HSD test, all statistics and comparison between other species and in situ planktonic communities are found in Figures S11–S12

used to model microalgae growth and dynamic physiological state (Geider, 1987). In *N. frigida* alone, we observed a break in the linear plot of C-to-Chl *a* against gE/gE_{opt} at $gE > 4\ gE_{opt}$ (Figure 3b), which could indicate severe photodamages under supersaturating irradiance for this shade-adapted sympagic species. Another surprising feature was the stabilization (and increase in *C. gelidus*) of C-to-Chl *a* as the *gE* was more limiting ($gE \approx 0.1gE_{opt}$) in four out of the five species examined, contrasting with the general trend in temperate diatoms (MacIntyre et al., 2002), although exceptions have been reported [e.g. *Skeletonema costatum*, Falkowski and Owens (1980)]. In the C-to-Chl *a* ratio range for which a linear increase as a function of *gE* intensity was observed, the steepest slopes were measured in *N. frigida* and *F. cylindrus* (Table 2), which indicate larger fluctuations in Chl *a* investment over narrow light intensity changes, as expected in shade-adapted organisms (notice also the lowest C-to-Chl *a* slope in *T. gravida* and *C. neogracilis*). However, the C-to-Chl *a* slopes versus gE/gE_{opt} were closer (although still clearly lower in *T. gravida*; Table 1), indicating similar regulations among species when expressed relative to their respective growth potential. The minimal ≈25 g·g^{-1} C-to-Chl *a* ratio to which species roughly converged under the most limiting *gE* intensity (more visible as the inverse ≈0.04 g·g^{-1} Chl *a*-to-C in Figure 3b) is similar to the extrapolated *y*-intercept observed in temperate diatoms (Lacour et al., 2017). However, we find here that C-to-Chl *a* values diverge from a linear model at the most limiting *gE* intensities, which could be ecologically relevant, particularly for sympagic diatoms which dominate in Arctic primarily when light intensity is extremely low (Hancke et al., 2018; Figure 1). An equilibrium at ≈25 g·g^{-1} C-to-Chl *a* is possibly reached between the minimal C quota for survival and as the 'return on investment' for synthesizing new Chl *a* saturates, because absorption per pigment molecule decreases beyond a threshold due to internal self-shading (Morel & Bricaud, 1981).

Despite unexpected variations in C-to-Chl *a* at very low *gE* intensity, we observed roughly stable α^* in this gE/gE_{opt} range (except in *F. cylindrus*), as expected because Chl *a* content correlates positively to photon delivery. However, under higher *gE*, but still below gE_{opt}, all species showed a similar decrease in α^* except *F. cylindrus* for which the decrease was steeper but for which α^* overshot to values at least 50% higher than any other species for equal intermediate gE/gE_{opt} (0.3–1; Figure 4a). Noteworthy, a constant ratio between α and Chl *a*

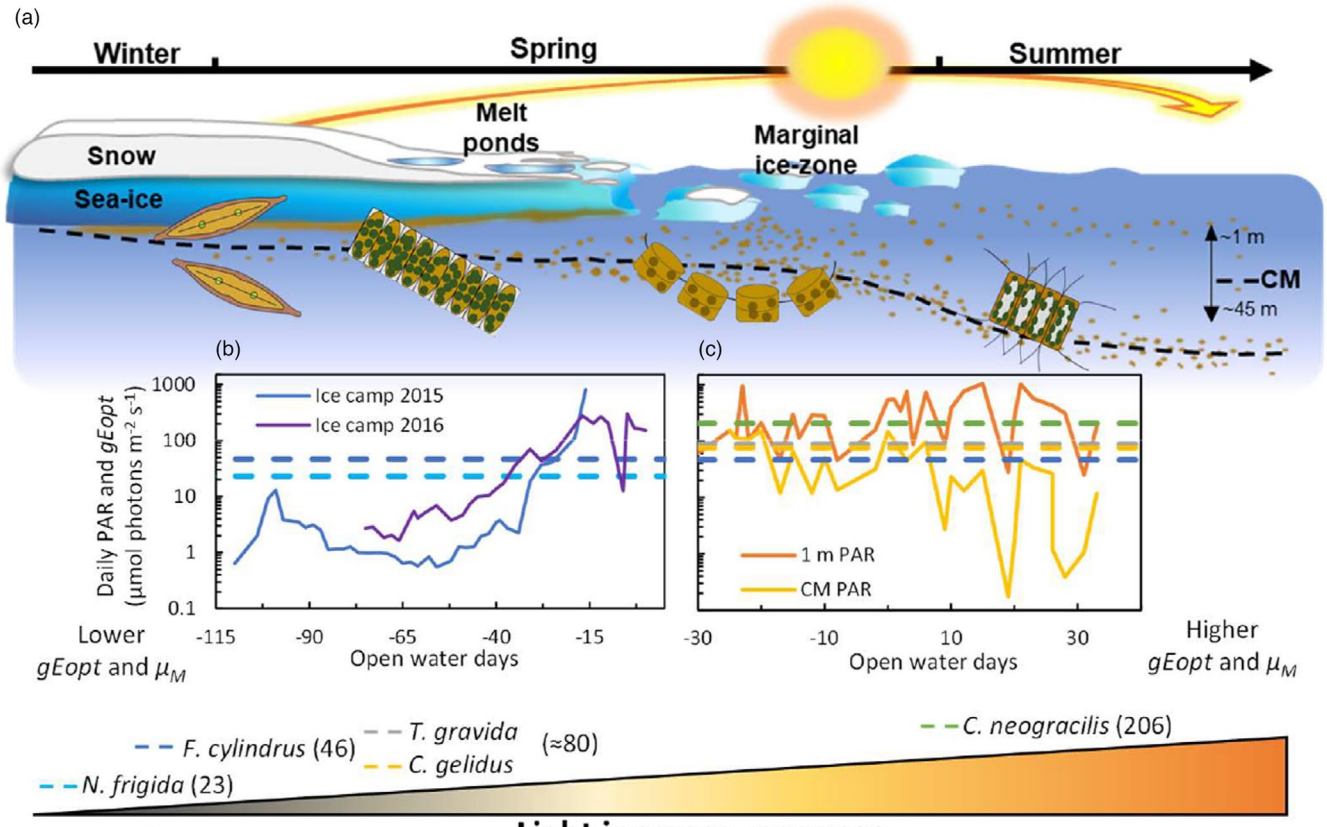

(d)

	Light increase response			
	Below *gEOpt*		Above *gEOpt*	
	LL specialist	HL specialist	LL specialist	HL specialist
μ	↑	↑	↓↓	≈
C-to-Chl *a*	≈	≈	↑	↑
α^*	≈	≈	↓	↓
P^*_M	↑	↑↑	≈	↑↑
P_{gE}	↑	↑	↓	↓
DES	↑	≈	↑↑	↑
F_V/F_M	≈	≈	↓↓	↓
σPSII	≈	≈	↓	↓

FIGURE 8 Synthesis figure of the interaction between Arctic diatoms photoacclimative response to the habitat and light environment shift over a typical spring-to-summer Arctic diatom succession in Baffin Bay (where the Green Edge campaigns were conducted) (a). Daily averaged photosynthetically available radiation (PAR) in µmol photons m^{-2} s^{-1} at the sea-ice-water interface during the 2015 and 2016 ice-camps (b), and at the water column surface (≈1 m) and at the chlorophyll *a* maximum (CM) (CM progressing depth is shown in Figure 1c) during the 2016 oceanographic campaign (c). Horizontal lines indicate studied Arctic species light intensity for maximal growth (gE_{opt}, in µmol photons m^{-2} s^{-1}), numerical and colour code are shown next to species name on the light gradient representation. The typical variations in photophysiological parameters upon *gE* intensity increased below or above growth saturation (above or below gE_{opt}) in low-light (LL) specialists (based on sympagic *Nitzschia frigida*) and in high-light (HL) specialists (based on open-water planktonic *Chaetoceros neogracilis*) (d). See Materials and Methods and Figure S1 for definition of the abbreviated parameters shown

content relies on strong assumptions, notably that both the photon/electron requirement per fixed C remain unvaried. In temperate species, the photosynthetic electron transport and the CBB cycle are expected to face no thermodynamic restrictions under the limiting light intensities defining α. However, this is possibly not the case for polar species as low temperature can impose constraints on C-fixation (Young et al., 2015), which could trigger acclimative processes remaining active while the samples are transferred to lower light for ^{14}C-uptake measurements, and thus affect α^*. Crucially, the earlier member of the succession, sympagic or planktonic more dominant in

the marginal ice zone, for which we previously reported important sustained NPQ in darkness and under sub-saturating light, *N. frigida*, *F. cylindrus* and *T. gravida* (Croteau et al., 2021; Lacour et al., 2018), developed DES twofold to threefold higher than in the *Chaetoceros* species under $gE < gE_{opt}$ (Figure 6d). Such light energy dissipated as heat would increase the photon requirement for C-fixation, hence lower α^*. A possible advantage of dissipating light energy via reversible NPQ at limiting light rather than by degrading Chl *a*, could be to maximize harvesting of weaker light intensities at lower solar angle over a daily cycle or when planktonic cells undergo deep mixing (when NPQ can be downregulated). This could be particularly crucial for sympagic species as from the onset of the snowmelt period, it takes <3 weeks for the average daily PAR to exceed *N. frigida*'s gE_{opt} (Figure 1b), highlighting the need to exploit daily periods of lower light (Lacour et al., 2020). Photodamages can also decrease α^* under intense *gE* (Marshall et al., 2000), but our data plotted as a function of gE/gE_{opt} indicate a lag between the decrease in α^* (Figure 4a) and the decrease in F_v/F_M (Figure 6a), suggesting photodamages could only explain lower α^* under the highest *gE* intensities. Downstream of photon absorption, various alternative electron fluxes can lead to ATP production without generating NADPH which increases the electron requirement for C-fixation (and decrease α^* if active under limiting light). These pathways are usually more active under high light and provide photoprotection (Wagner et al., 2016), but not always, as for instance cyclic electron flow around PSI is constitutive in green organisms (Munekage et al., 2004), a pathway suspected of having an enhanced rate in *F. cylindrus* compared to temperate diatom counterparts (Goldman et al., 2015). Interestingly, Kulk et al. (2019), described a 2.5-fold increase in electron requirement per C fixed under limiting growth light in two out of four Antarctic diatom species, including *Fragilariopsis* sp. Coinciding with *F. cylindrus* being the only species for which we observed decreasing α^* under the lowest *gE* in this study.

4.2 | Contrasts in C-specific productivity among species and depending upon growth light intensity

Data on C-specific ^{14}C-uptake also reflected a photoadaptation gradient, with the lowest P^C_M in sympagic *N. frigida* and maximal P^C_M in open-water *C. neogracilis*. In a deviation from a straightforward gradient of species of increasing productivity along the habitat seasonal transformation, maximal P^C_M was higher in dual sympagic/planktonic *F. cylindrus* than in marginal ice zone dominant *T. gravida* and open-water *C. gelidus*. Nonetheless, as for other parameters in *F. cylindrus*, P^C_M varied drastically depending upon *gE*, reflecting this species optimal performance under a very narrow range of *gE*. We extrapolated the 20 min ^{14}C-uptake under *gE* to 24 hr (P_{gE}) to compare it to species growth rates (net production). It can be contentious to use short ^{14}C-incubation to gauge gross-to-net production because photosynthates are allocated to different metabolic pools (Milligan et al., 2015) with different turnover rates. However, we believe it is reasonable to use 20 min ^{14}C-uptake to compare trends in P_{gE} over a large *gE*/*gEopt* range with parallel measurements of growth rates, to distinguish photoadaptative features between species (Figure 5). Both *F. cylindrus* and *C. neogracilis* showed higher maximal P_{gE} than the other species, possibly reflecting high investment in Rubisco (Goldman et al., 2015; Young et al., 2015). But strikingly, high C-fixation only converted into higher growth rates in *C. neogracilis* [i.e. high growth efficiency (η_g, Equation 11)], showing that if elevated CBB capacity is a prerequisite for fast growth rates (Behrenfeld et al., 2021), it is not necessarily sufficient. Halsey et al. (2010, 2011) showed that photosynthates partitioning between pools of short lifetimes respired for energy balance, and long lifetimes used for growth, vary between species. Yet, the partitioning generally trends towards longer lifetime metabolites as growth rates approach μ_M and more cells in the population are in division phase at a given moment, yielding ^{14}C measurements closer to net production (higher η_g; Milligan et al., 2015). Except for the lowest *gE* intensity in *F. cylindrus*, our results generally agree with this model, although it seems like the highest η_g were reached past μ_M, when growth rates began to be photoinhibited for the earlier species of the succession (more in *N. frigida* and *F. cylindrus* than in *T. gravida*; Figure 6d). It is possible that some cells died under supersaturating light and that an increased in underlying death rate led to an underestimation of μ_M when η_g peaked towards ≈1. We noticed empty frustules under the two highest *gE* intensities when counting *N. frigida* by inverted microscopy, but we could not accurately estimate death rates. More acute photoinhibition in sea-ice/dual-form pennate species (*N. frigida* and *F. cylindrus*) compared to centric planktonic species may be due to expanded upregulation of the reactive oxygen species scavenging machinery under high light stress in the former (Kvernvik et al., 2020). Interestingly, we noticed an inverse linear relationship between η_g and α^* ($R^2 = 0.51$) and P^C_M ($R^2 = 0.45$; Figure S8). This might indicate that when photosynthates are mostly allocated to growth (increasing η_g), upregulation of alternative electron fluxes overtake energy balance rather than chloroplast to mitochondrion shuffling (decreasing α^* and P^C_M; Bailleul et al., 2015).

4.3 | Comparison between laboratory and in situ ^{14}C-uptake curves

Next, to validate that the contrasts between sympagic and planktonic species are representative of in situ dynamics, we compared it to α^* and P^*_M monitored over the Green Edge campaigns (Oziel et al., 2019; Randelhoff et al., 2019; Massicotte et al., 2020; Figure 7). Field measurements supported our findings, with significantly higher α^* and P^C_M in natural planktonic communities compared to sympagic ones ($p < 0.001$, Figure 7a,b). Moreover, the responses of α^* and P^C_M as a function of in situ *gE*/PAR intensities were much alike between sympagic *N. frigida*, and in situ sympagic communities although it diverged from what is expected in temperate diatoms (MacIntyre et al., 2002). Planktonic samples did not show any significant differences when regrouped by LH (Figure S12) possibly

because of greater and stochastic (as opposed to progressively driven by snowmelt) daily variations in light availability (Figure 1c,d) muddling photoacclimation patterns, shifts in assemblages composition (Figure S3) and/or decreasing nutrients stocks post-bloom (Krause et al., 2019; Lafond et al., 2019). Nevertheless, despite its simplicity (notably considering daily PAR at a single depth without integrating vertical mixing), this comparative approach confirms that laboratory measurements on species relevant to the ecological niche sampled are in the range of field measurements on natural assemblages.

4.4 | Specialists versus generalist photoadaptation and trade-offs with other environmental pressures

We linked the contrasted responses of succession endmembers *N. frigida* and *C. neogracilis* to low-light and high-light specialists respectively (Figure 8). By comparison, the intermediate responses of *F. cylindrus*, *T. gravida* and *C. gelidus* can be seen as more generalist photoadaptation. This raises the question at to the potential trade-offs between specialist and generalist photoadaptation strategies in natural conditions? We proposed *N. frigida* evolved a survivalist strategy related to its extreme environment, characterized by nutrient stresses, hyperoxia, sub-zero temperatures and osmotic shocks (Thomas & Dieckmann, 2002) overlapping with large shifts in PAR (Figure 1b). Sympagic species express extensive molecular machinery to cope with environmental stresses (Mock et al., 2017), and allocate important resources to protective exopolysaccharides (Krembs et al., 2011) and ice-binding proteins (Janech et al., 2006), which improve their survivability in sea-ice rather than increasing productivity. Considering *N. frigida* dominance in Arctic sea-ice (≈60% of cell counts in our data (Figure 1d), see also Poulin et al., 2011), it is tempting to suggest its photoadaptive plasticity reflects a near-optimal balance between strong resilience against stress with limited potential gross productivity in in situ sea-ice conditions. Intriguingly, while *N. frigida* is clearly less productive and more photoinhibited under supersaturating *gE* (also visible in sympagic/planktonic *F. cylindrus*) than planktonic species, no evidence supports ice-related photoadaptation as being advantageous under lower growth light intensity (see the initial slope of light-limited growth rate (Figure 2e), *PgE* under low *gE* (Figure 5b) and similar conclusions reached by Kvernvik et al. (2021). Arctic spring time means low light intensities but also very short photoperiods, and variations in diatoms' growth rates as a function of photoperiod are species dependent (Li et al., 2017; Shatwell et al., 2013). An important hypothesis to test, by covarying photoperiod length and growth light intensity, is whether, compared to planktonic species, ice-related species evolved optimized opportunistic utilization of short-lived light doses.

The contrasting high-light specialist strategy of *C. neogracilis* raises other questions: Why does *C. neogracilis* not dominate over the other species in natural conditions? Or perhaps, why have the other species have not evolved similar high-productivity-oriented strategies? One partial answer may come from light niche and depth adaptation. *Chaetoceros* species are not as much associated with less intensely lit ice-covered waters than *Fragilariopsis* or *Thalassiosira* (Lafond et al., 2019; Poulin et al., 2011). Moreover, *C. gelidus* often colonizes the deep chlorophyll maximum while *C. neogracilis* typically dwell in more intensely illuminated surficial waters (Balzano et al., 2012, 2017). The strains used were isolated from these contrasted depths, which has been documented to influence photoadaptation (Bailey et al., 2005). However, diatom blooms are not strictly dependent upon the fastest growth rates but are rather driven by imbalances between photosynthetic growth, grazing (Behrenfeld et al., 2017) and sinking. *Chaetoceros neogracilis* is the smallest species of our study and is most often found in solitary cells, in opposition to all other species which form colonies of dozens of cells (Balzano et al., 2017; von Quillfeldt, 2000). In diatoms, both larger cellular volume (Smetacek et al., 2004) and colony size, which can increase in the presence of predators (Bergkvist et al., 2012), seem to reduce population susceptibility to grazing. Recently, Behrenfeld et al. (2021) challenged the traditional view of an allometric limit to the maximal growth rates of larger cells and proposed instead that smaller/solitary taxa might have been 'forced' to evolve faster growth rates to outgrow predation, which could explain the photoadaptation strategy observed here in *C. neogracilis*. As for the molecular adaptation underpinning faster growth rates in *C. neogracilis* even with P_{gE} similar to other species (Figure 5), it is possible *C. neogracilis* invests more in phosphorus-rich division machinery (Klausmeier et al., 2004). Elemental stoichiometry of nine polar species revealed lower N:P ratios in the *Thalassiosira* genus (Lomas et al., 2019), which are important bloomers in the Arctic (Arrigo et al., 2012; Balzano et al., 2017; Booth et al., 2002), but the study did not include *Chaetoceros* representatives (nor *Fragilariopsis* nor *Nitzschia*). Interestingly, an earlier study on Arctic diatoms (Sakshaug et al., 1991) focused on *Chaetoceros furcellatus* and *Thalassiosira nordenskioeldii*, typical of late Arctic seasonal succession (Luddington et al., 2016; Poulin et al., 2011). In Sakshaug et al. (1991), both species showed barely lower α^* and higher P^*_M when grown under 400 rather than 25 μmol photons m^{-2} s^{-1}, much like *C. neogracilis* and *T. gravida* here. However, *C. furcellatus* and *T. nordenskioeldii*, which both form colonies, showed maximal growth rates much closer to *T. gravida* (≈0.33 d^{-1}) than *C. neogracilis* (≈0.66 d^{-1}). This reinforces the importance of integrating species representative of diverse niches for comprehensive description of ecological dynamics, as previously reported in temperate planktonic (Lavaud et al., 2007, Fisher et al., 2020) and microphytobenthos (Barnett et al., 2015) diatoms.

5 | CONCLUSIONS

This study highlights that a shift in optimal light for growth across Arctic diatom taxa aligns with their seasonal succession during spring bloom, and that species found later in the succession are more productive and less sensitive to photoinhibition. Moreover, we revealed that many key assumptions regarding phytoplankton

responses to light availability in models (linear increases in C-to-Chl *a* and P^*_M, and phenotypically invariant α^* and P^C_M under ranging growth lights) are oversimplifications with regards to Arctic diatom diversity. This is especially true under limiting and supersaturating light conditions, which are inherent to the Arctic Ocean seasonal cycle. These results will be useful to improve productivity models and anticipate perturbations of diatoms succession dynamics in the rapidly changing Arctic Ocean. A more intense light environment with less ice (Lewis et al., 2020) should favour higher μ_M strategist (Behrenfeld et al., 2021) like *C. neogracilis*, but trade-offs with other factors in the natural context, including photoperiod regime, grazing pressure and nutrient availability need to be further investigated. Variations in primary production curves are often reported between different water masses (ice-covered vs. ice-free) in Arctic oceanographic campaigns but mostly interpreted as due to varying environmental conditions (Lewis et al., 2019; Schuback et al., 2017; Zhu et al., 2019). Additionally, we show here by comparing laboratory and in situ data, that a niche-resolved approach can also yield valuable insights. To better comprehend ecological perturbations in the rapidly changing Arctic Ocean, we reckon it is essential to factor in both environmental parameters and niche adaptation (Caracciolo et al., 2021).

ACKNOWLEDGEMENTS

We thank the contribution of CNRS in the framework of the IRL Takuvik, the Canada Excellence Research Chair on Remote sensing of Canada's new Arctic frontier (M. Babin), NSERC Canada Discovery grant (RGPIN-2017-04505; J. Lavaud), the Sentinel North program of Université Laval (Canada First Research Excellence Fund) and the research network Québec-Océan for their financial support; J. Larivière and M. Béguin for their technical support; M. Simard and V. Richard for their support with HPLC analyses; P. Massicotte for his help with Figure S2 and statistical analysis; and Profs. A. Juhl for kindly providing us with the *N. frigida* strain. The project Green Edge was conducted under the scientific coordination of the Canada Excellence Research Chair on Remote sensing of Canada's new Arctic frontier, and the CNRS and Université Laval Takuvik International Research Laboratory (IRL3376). We thank officers and crew of CCGS *Amundsen* and Marie-Hélène Forget, and Joannie Ferland for planning the field work, and all other scientists and technicians involved in the Green Edge campaigns for their contribution to field work and data collection. In particular, Tonya Burgers and Brent Else kindly provided the shipboard PAR measurements. We also thank Québec-Océan and the Polar Continental Shelf Program for their in-kind contribution in terms of polar logistics and scientific equipment. The GreenEdge project was funded by the following French and Canadian programs and agencies: ANR (Contract #111112), ArcticNet, CERC on Remote sensing of Canada's new Arctic frontier, CNES (project #131425), French Arctic Initiative, Fondation Total, CSA, LEFE and IPEV (project #1164). This project was conducted using the Canadian research icebreaker CCGS *Amundsen* with the support of the Amundsen Science program funded by the Canada Foundation for Innovation (CFI) Major Science Initiatives (MSI) Fund.

CONFLICT OF INTEREST

The authors have no conflict of interests to declare.

AUTHORS' CONTRIBUTIONS

D.C., T.L., N.S., J.-É.T., D.A.C., M.B. and J.L. conceived the ideas and designed the laboratory methodology; D.C., T.L., N.S., P.-I.M., F.B. and J.F. collected the laboratory data; M.B., conceived and designed the Green Edge project; J.F. and M.-H.F. conducted field photosynthetic curves; A.L. realized field sampling and taxonomy; D.C., T.L., N.S., D.A.C. and J.L. analysed the data; D.C. and J.L. led the writing of the manuscript; all authors contributed critically to the drafts and gave final approval for publication.

PEER REVIEW

The peer review history for this article is available at https://publons.com/publon/10.1111/1365-2745.13874.

DATA AVAILABILITY STATEMENT

The data presented in the manuscript are archived as a data package on Dryad Digital Repository https://doi.org/10.5061/dryad.sn02v6x65 (Croteau et al., 2022). All data collected over the Green Edge project are available at http://www.obs-vlfr.fr/proof/php/GREENEDGE/greenedge.php (Massicotte et al., 2020).

ORCID

Dany Croteau https://orcid.org/0000-0001-9322-8634
Thomas Lacour https://orcid.org/0000-0003-2295-6188
Douglas A. Campbell https://orcid.org/0000-0001-8996-5463
Johann Lavaud https://orcid.org/0000-0002-4704-2502

REFERENCES

Alou-Font, E., Mundy, C. J., Roy, S., Gosselin, M., & Agustí, S. (2013). Snow cover affects ice algal pigment composition in the coastal Arctic Ocean during spring. *Marine Ecology Progress Series*, *474*, 89–104. https://doi.org/10.3354/meps10107

Ardyna, M., Mundy, C. J., Mills, M. M., Oziel, L., Grondin, P.-L., Lacour, L., Verin, G., van Dijken, G., Ras, J., Alou-Font, E., Babin, M., Gosselin, M., Tremblay, J.-É., Raimbault, P., Assmy, P., Nicolaus, M., Claustre, H., & Arrigo, K. R. (2020). Environmental drivers of under-ice phytoplankton bloom dynamics in the Arctic Ocean. *Elementa: Science of the Anthropocene*, *8*. https://doi.org/10.1525/elementa.430

Arrigo, K. R., Perovich, D. K., Pickart, R. S., Brown, Z. W., van Dijken, G. L., Lowry, K. E., Mills, M. M., Palmer, M. A., Balch, W. M., Bahr, F., Bates, N. R., Benitez-Nelson, C., Bowler, B., Brownlee, E., Ehn, J. K., Frey, K. E., Garley, R., Laney, S. R., Lubelczyk, L., … Swift, J. H. (2012). Massive phytoplankton blooms under Arctic Sea Ice. *Science*, *336*(6087), 1408. https://doi.org/10.1126/science.1215065

Aumack, C. F., & Juhl, A. R. (2015). Light and nutrient effects on the settling characteristics of the sea ice diatom *Nitzschia frigida*. *Limnology and Oceanography*, *60*(3), 765–776. https://doi.org/10.1002/lno.10054

Babin, M. (2019). The phytoplankton spring bloom in the Arctic Ocean: Past, present and future response to climate variations, and impact on carbon fluxes and the marine food web. Elementa: Science of

the Anthropocene, 7. https://online.ucpress.edu/elementa/pages/green-edge

Bailey, S., Mann, N. H., Robinson, C., & Scanlan, D. J. (2005). The occurrence of rapidly reversible non-photochemical quenching of chlorophyll a fluorescence in cyanobacteria. *FEBS Letters*, *579*(1), 275–280. https://doi.org/10.1016/j.febslet.2004.11.091

Bailleul, B., Berne, N., Murik, O., Petroutsos, D., Prihoda, J., Tanaka, A., Villanova, V., Bligny, R., Flori, S., Falconet, D., Krieger-Liszkay, A., Santabarbara, S., Rappaport, F., Joliot, P., Tirichine, L., Falkowski, P. G., Cardol, P., Bowler, C., & Finazzi, G. (2015). Energetic coupling between plastids and mitochondria drives CO_2 assimilation in diatoms. *Nature*, *524*(7565), 366–369. https://doi.org/10.1038/nature14599

Balzano, S., Marie, D., Gourvil, P., & Vaulot, D. (2012). Composition of the summer photosynthetic pico and nanoplankton communities in the Beaufort Sea assessed by T-RFLP and sequences of the 18S rRNA gene from flow cytometry sorted samples. *ISME Journal*, *6*(8), 1480–1498. https://doi.org/10.1038/ismej.2011.213

Balzano, S., Percopo, I., Siano, R., Gourvil, P., Chanoine, M., Marie, D., Vaulot, D., & Sarno, D. (2017). Morphological and genetic diversity of Beaufort Sea diatoms with high contributions from the *Chaetoceros neogracilis* species complex. *Journal of Phycology*, *53*(1), 161–187. https://doi.org/10.1111/jpy.12489

Barnett, A., Méléder, V., Blommaert, L., Lepetit, B., Gaudin, P., Vyverman, W., Sabbe, K., Dupuy, C., & Lavaud, J. (2015). Growth form defines physiological photoprotective capacity in intertidal benthic diatoms. *The ISME Journal*, *9*(1), 32–45. https://doi.org/10.1038/ismej.2014.105

Behrenfeld, M. J., Halsey, K. H., Boss, E., Karp-Boss, L., Milligan, A. J., & Peers, G. (2021). Thoughts on the evolution and ecological niche of diatoms. *Ecological Monographs*, *91*(3). https://doi.org/10.1002/ecm.1457

Behrenfeld, M. J., Hu, Y., O'Malley, R. T., Boss, E. S., Hostetler, C. A., Siegel, D. A., Sarmiento, J. L., Schulien, J., Hair, J. W., Lu, X., Rodier, S., & Scarino, A. J. (2017). Annual boom–bust cycles of polar phytoplankton biomass revealed by space-based lidar. *Nature Geoscience*, *10*(2), 118–122. https://doi.org/10.1038/ngeo2861

Bergkvist, J., Thor, P., Jakobsen, H. H., Wängberg, S. Å., & Selander, E. (2012). Grazer-induced chain length plasticity reduces grazing risk in a marine diatom. *Limnology and Oceanography*, *57*(1), 318–324. https://doi.org/10.4319/lo.2012.57.1.0318

Blais, M., Ardyna, M., Gosselin, M., Dumont, D., Bélanger, S., Tremblay, J.-É., Gratton, Y., Marchese, C., & Poulin, M. (2017). Contrasting interannual changes in phytoplankton productivity and community structure in the coastal Canadian Arctic Ocean. *Limnology and Oceanography*, *62*(6), 2480–2497. https://doi.org/10.1002/lno.10581

Booth, B. C., Larouche, P., Bélanger, S., Klein, B., Amiel, D., & Mei, Z. P. (2002). Dynamics of *Chaetoceros socialis* blooms in the north water. *Deep-Sea Research Part II: Topical Studies in Oceanography*, *49*(22–23), 5003–5025. https://doi.org/10.1016/S0967-0645(02)00175-3

Bouman, H. A., Platt, T., Doblin, M., Figueiras, F. G., Gudmundsson, K., Gudfinnsson, H. G., Huang, B., Hickman, A., Hiscock, M., Jackson, T., Lutz, V. A., Mélin, F., Rey, F., Pepin, P., Segura, V., Tilstone, G. H., van Dongen-Vogels, V., & Sathyendranath, S. (2018). Photosynthesis–irradiance parameters of marine phytoplankton: Synthesis of a global data set. *Earth System Science Data*, *10*(1), 251–266. https://doi.org/10.5194/essd-10-251-2018

Buck, J. M., Sherman, J., Bártulos, C. R., Serif, M., Halder, M., Henkel, J., Falciatore, A., Lavaud, J., Gorbunov, M. Y., Kroth, P. G., Falkowski, P. G., & Lepetit, B. (2019). Lhcx proteins provide photoprotection via thermal dissipation of absorbed light in the diatom *Phaeodactylum tricornutum*. *Nature Communications*, *10*(1). https://doi.org/10.1038/s41467-019-12043-6

Campbell, K., Mundy, C. J., Juhl, A. R., Dalman, L. A., Michel, C., Galley, R. J., Else, B. E., Geilfus, N. X., & Rysgaard, S. (2019). Melt procedure affects the photosynthetic response of sea ice algae. *Frontiers in Earth Science*, *7*. https://doi.org/10.3389/feart.2019.00021

Caracciolo, M., Beaugrand, G., Hélaouët, P., Gevaert, F., Edwards, M., Lizon, F., Kléparski, L., & Goberville, E. (2021). Annual phytoplankton succession results from niche-environment interaction. *Journal of Plankton Research*, *43*(1), 85–102. https://doi.org/10.1093/plankt/fbaa060

Chang, C. C., Halpern, C. B., Antos, J. A., Avolio, M. L., Biswas, A., Cook, J. E., del Moral, R., Fischer, D. G., Holz, A., Pabst, R. J., Swanson, M. E., & Zobel, D. B. (2019). Testing conceptual models of early plant succession across a disturbance gradient. *Journal of Ecology*, *107*(2), 517–530. https://doi.org/10.1111/1365-2745.13120

Croteau, D., Guérin, S., Bruyant, F., Ferland, J., Campbell, D. A., Babin, M., & Lavaud, J. (2021). Contrasting nonphotochemical quenching patterns under high light and darkness aligns with light niche occupancy in Arctic diatoms. *Limnology and Oceanography*, *66*(S1), S231–S245. https://doi.org/10.1002/lno.11587

Croteau, D., Lacour, T., Schiffrine, N., Morin, P.-I., Forget, M.-H., Bruyant, F., Ferland, J., Lafond, A., Campbell, D. A., Tremblay, J.-É., Babin, M., & Lavaud, J. (2022). Data from: Shifts in growth light optima among diatom species support their succession during the spring bloom in the Arctic. Dryad Digital Repository, https://doi.org/10.5061/dryad.sn02v6x65

Dubinsky, Z., & Stambler, N. (2009). Photoacclimation processes in phytoplankton: Mechanisms, consequences, and applications. *Aquatic Microbial Ecology*, *56*, 163–176. https://doi.org/10.3354/ame01345

Eilers, P. H. C., & Peeters, J. C. H. (1988). A model for the relationship between light intensity and the rate of photosynthesis in phytoplankton. *Ecological Modelling*, *42*(3–4), 199–215. https://doi.org/10.1016/0304-3800(88)90057-9

Falkowski, P. G., & Owens, T. G. (1980). Light—Shade adaptation. *Plant Physiology*, *66*(4), 592–595. https://doi.org/10.1104/pp.66.4.592

Fisher, N. L., Campbell, D. A., Hughes, D. J., Kuzhiumparambil, U., Halsey, K. H., Ralph, P. J., & Suggett, D. J. (2020). Divergence of photosynthetic strategies amongst marine diatoms. *PLoS ONE*, *15*(12), e0244252. https://doi.org/10.1371/journal.pone.0244252

Galindo, V., Gosselin, M., Lavaud, J., Mundy, C. J., Else, B., Ehn, J., Babin, M., & Rysgaard, S. (2017). Pigment composition and photoprotection of Arctic sea ice algae during spring. *Marine Ecology Progress Series*, *585*, 49–69. https://doi.org/10.3354/meps12398

Geider, R. J. (1987). Light and temperature dependence of the carbon to chlorophyll a ratio in microalgae and cyanobacteria: Implications for physiology and growth of phytoplankton. *New Phytologist*, *106*(1), 1–34. https://doi.org/10.1111/j.1469-8137.1987.tb04788.x

Geider, R. J., MacIntyre, H. L., & Kana, T. M. (1998). A dynamic regulatory model of phytoplanktonic acclimation to light, nutrients, and temperature. *Limnology and Oceanography*, *43*(4), 679–694. https://doi.org/10.4319/lo.1998.43.4.0679

Goldman, J. A. L., Kranz, S. A., Young, J. N., Tortell, P. D., Stanley, R. H. R., Bender, M. L., & Morel, F. M. M. (2015). Gross and net production during the spring bloom along the Western Antarctic peninsula. *New Phytologist*, *205*(1), 182–191. https://doi.org/10.1111/nph.13125

Halsey, K. H., Milligan, A. J., Behrenfeld, M. J., Halsey, K. H., Milligan, A. J., & Behrenfeld, M. J. (2010). Physiological optimization underlies growth rate-independent chlorophyll-specific gross and net primary production. *Photosynthesis Research*, *103*(2), 125–137. https://doi.org/10.1007/s11120-009-9526-z

Halsey, K. H., Milligan, A. J., & Behrenfeld, M. J. (2011). Linking time-dependent carbon-fixation efficiencies in *Dunaliella tertiolecta* (Chlorophyceae) to underlying metabolic pathways. *Journal of Phycology*, *47*(1), 66–76. https://doi.org/10.1111/j.1529-8817.2010.00945.x

Hancke, K., Lund-Hansen, L. C., Lamare, M. L., Højlund Pedersen, S., King, M. D., Andersen, P., & Sorrell, B. K. (2018). Extreme low light requirement for algae growth underneath sea ice: A case study from station Nord, NE Greenland. *Journal of Geophysical Research:*

Oceans, *123*(2), 985–1000. https://doi.org/10.1002/2017JC013263

Hooker, S. B., Morrow, J. H., & Matsuoka, A. (2013). Apparent optical properties of the Canadian Beaufort Sea – Part 2: The 1% and 1 cm perspective in deriving and validating AOP data. *Biogeosciences*, *10*(7), 4511–4527. https://doi.org/10.5194/bg-10-4511-2013

Janech, M. G., Krell, A., Mock, T., Kang, J. S., & Raymond, J. A. (2006). Ice-binding proteins from sea ice diatoms (Bacillariophyceae). *Journal of Phycology*, *42*(2), 410–416. https://doi.org/10.1111/j.1529-8817.2006.00208.x

Katlein, C., Perovich, D. K., & Nicolaus, M. (2016). Geometric effects of an Inhomogeneous Sea ice cover on the under ice light field. *Frontiers in Earth Science*, *4*(February), 2–11. https://doi.org/10.3389/feart.2016.00006

Klausmeier, C. A., Litchman, E., Daufreshna, T., & Levin, S. A. (2004). Optimal nitrogen-to-phosphorus stoichiometry of phytoplankton. *Nature*, *429*(6988), 171–174. https://doi.org/10.1038/nature02454

Koch, C. W., Cooper, L. W., Grebmeier, J. M., Frey, K., & Brown, T. A. (2020). Ice algae resource utilization by benthic macro- and megafaunal communities on the Pacific Arctic shelf determined through lipid biomarker analysis. *Marine Ecology Progress Series*, *651*, 23–43. https://doi.org/10.3354/meps13476

Krause, J. W., Schulz, I. K., Rowe, K. A., Dobbins, W., Winding, M. H. S., Sejr, M. K., Duarte, C. M., & Agustí, S. (2019). Silicic acid limitation drives bloom termination and potential carbon sequestration in an Arctic bloom. *Scientific Reports*, *9*(1). https://doi.org/10.1038/s41598-019-44587-4

Krembs, C., Eicken, H., & Deming, J. W. (2011). Exopolymer alteration of physical properties of sea ice and implications for ice habitability and biogeochemistry in a warmer Arctic. *Proceedings of the National Academy of Sciences of the United States of America*, *108*(9), 3653–3658. https://doi.org/10.1073/pnas.1100701108

Kulk, G., Buist, A., van de Poll, W. H., Rozema, P. D., & Buma, A. G. J. (2019). Size scaling of photophysiology and growth in four freshly isolated diatom species from Ryder Bay, western Antarctic peninsula. *Journal of Phycology*, *328*, 314–328. https://doi.org/10.1111/jpy.12813

Kvernvik, A. C., Hoppe, C. J. M., Greenacre, M., Verbiest, S., Wiktor, J. M., Gabrielsen, T. M., Reigstad, M., & Leu, E. (2021). Arctic sea ice algae differ markedly from phytoplankton in their ecophysiological characteristics. *Marine Ecology Progress Series*, *666*, 31–55. https://doi.org/10.3354/meps13675

Kvernvik, A. C., Rokitta, S. D., Leu, E., Harms, L., Gabrielsen, T. M., Rost, B., & Hoppe, C. J. M. (2020). Higher sensitivity towards light stress and ocean acidification in an Arctic Sea-ice-associated diatom compared to a pelagic diatom. *New Phytologist*, *226*(6), 1708–1724. https://doi.org/10.1111/nph.16501

Lacour, T., Babin, M., & Lavaud, J. (2020). Diversity in xanthophyll cycle pigments content and related nonphotochemical quenching (NPQ) among microalgae: Implications for growth strategy and ecology. *Journal of Phycology*, *56*(2), 245–263. https://doi.org/10.1111/jpy.12944

Lacour, T., Larivière, J., & Babin, M. (2017). Growth, Chl *a* content, photosynthesis, and elemental composition in polar and temperate microalgae. *Limnology and Oceanography*, *62*(1), 43–58. https://doi.org/10.1002/lno.10369

Lacour, T., Larivière, J., Ferland, J., Bruyant, F., Lavaud, J., & Babin, M. (2018). The role of sustained photoprotective non-photochemical quenching in low temperature and high light acclimation in the bloom-forming Arctic diatom *Thalassiosira gravida*. *Frontiers in Marine Science*, *5*(October), 1–16. https://doi.org/10.3389/fmars.2018.00354

Lafond, A., Leblanc, K., Quéguiner, B., Moriceau, B., Leynaert, A., Cornet, V., Legras, J., Ras, J., Parenteau, M., Garcia, N., Babin, M., & Tremblay, J.-É. (2019). Late spring bloom development of pelagic diatoms in Baffin Bay. *Elementa: Science of the Anthropocene*, *7*, 44. https://doi.org/10.1525/elementa.382

Lavaud, J., Strzepek, R. F., & Kroth, P. G. (2007). Photoprotection capacity differs among diatoms: Possible consequences on the spatial distribution of diatoms related to fluctuations in the underwater light climate. *Limnology and Oceanography*, *52*(3), 1188–1194. https://doi.org/10.4319/lo.2007.52.3.1188

Leu, E., Mundy, C. J., Assmy, P., Campbell, K., Gabrielsen, T. M., Gosselin, M., Juul-Pedersen, T., & Gradinger, R. (2015). Arctic spring awakening – Steering principles behind the phenology of vernal ice algal blooms. *Progress in Oceanography*, *139*, 151–170. https://doi.org/10.1016/j.pocean.2015.07.012

Leu, E., Graeve, M., & Wulff, A. (2016). A (too) bright future? Arctic diatoms under radiation stress. *Polar Biology*, *39*(10), 1711–1724. https://doi.org/10.1007/s00300-016-2003-1

Lewis K. M., Arntsen A. E., Coupel P., Joy-Warren H., Lowry K. E., Matsuoka A., Mills M. M., Dijken G. L., Selz V., Arrigo K. R. (2019). Photoacclimation of Arctic Ocean phytoplankton to shifting light and nutrient limitation. *Limnology and Oceanography*, *64*(1), 284.–301. https://doi.org/10.1002/lno.11039

Lewis, K. M., van Dijken, G. L., & Arrigo, K. R. (2020). Changes in phytoplankton concentration now drive increased Arctic Ocean primary production. *Science*, *369*(6500), 198–202. https://doi.org/10.5194/bg-2019-289

Li, G., Talmy, D., Campbell, D. A. (2017). Diatom growth responses to photoperiod and light are predictable from diel reductant generation. *Journal of phycology*, *53*(1), 95–107. https://doi.org/10.1111/jpy.12483

Lomas, M. W., Baer, S. E., Acton, S., & Krause, J. W. (2019). Pumped up by the cold: Elemental quotas and stoichiometry of cold-water diatoms. *Frontiers in Marine Science*, *6*(June), 286. https://doi.org/10.3389/fmars.2019.00286

Losa, S. N., Dutkiewicz, S., Losch, M., Oelker, J., Soppa, M. A., Trimborn, S., Xi, H., & Bracher, A. (2019). On modeling the Southern Ocean phytoplankton functional types. *Biogeosciences Discussions*, (July), 1–37. https://doi.org/10.5194/bg-2019-289

Luddington, I. A., Lovejoy, C., & Kaczmarska, I. (2016). Species-rich metacommunities of the diatom order Thalassiosirales in the Arctic and northern Atlantic Ocean. *Journal of Plankton Research*, *38*(4), 781–797. https://doi.org/10.1093/plankt/fbw030

Luostarinen, T., Ribeiro, S., Weckström, K., Sejr, M., Meire, L., Tallberg, P., & Heikkilä, M. (2020). An annual cycle of diatom succession in two contrasting Greenlandic fjords: From simple sea-ice indicators to varied seasonal strategists. *Marine Micropaleontology*, *158*(March), 101873. 101873. https://doi.org/10.1016/j.marmicro.2020.101873

MacIntyre, H. L., Kana, T. M., Anning, T., & Geider, R. J. (2002). Photoacclimation of photosynthesis irradiance response curves and photosynthetic pigments in microalgae and cyanobacteria. *Journal of Phycology*, *38*(1), 17–38. https://doi.org/10.1046/j.1529-8817.2002.00094.x

Marshall, H. L., Geider, R. J., & Flynn, K. J. (2000). A mechanistic model of photoinhibition. *New Phytologist*, *145*(2), 347–359. https://doi.org/10.1046/j.1469-8137.2000.00575.x

Massicotte, P., Amiraux, R., Amyot, M.-P., Archambault, P., Ardyna, M., Arnaud, L., Artigue, L., Aubry, C., Ayotte, P., Bécu, G., Bélanger, S., Benner, R., Bittig, H. C., Bricaud, A., Brossier, É., Bruyant, F., Chauvaud, L., Christiansen-Stowe, D., Claustre, H., … Babin, M. (2020). Green Edge ice camp campaigns: Understanding the processes controlling the under-ice Arctic phytoplankton spring bloom. *Earth System Science Data*, *12*(1), 151–176. https://doi.org/10.5194/essd-12-151-202

Milligan, A. J., Halsey, K. H., & Behrenfeld, M. J. (2015). HORIZONS: Advancing interpretations of ^{14}C-uptake measurements in the context of phytoplankton physiology and ecology. *Journal of*

Plankton Research, *37*(4), 692–698. https://doi.org/10.1093/plankt/fbv051

Mock, T., Otillar, R. P., Strauss, J., McMullan, M., Paajanen, P., Schmutz, J., Salamov, A., Sanges, R., Toseland, A., Ward, B. J., Allen, A. E., Dupont, C. L., Frickenhaus, S., Maumus, F., Veluchamy, A., Wu, T., Barry, K. W., Falciatore, A., Ferrante, M. I., … Grigoriev, I. V. (2017). Evolutionary genomics of the cold-adapted diatom *Fragilariopsis cylindrus*. *Nature*, *541*(7638), 536–540. https://doi.org/10.1038/nature20803

Morel, A., & Bricaud, A. (1981). Theoretical results concerning light absorption in a discrete medium, and application to specific absorption of phytoplankton. *Deep Sea Research Part A. Oceanographic Research Papers*, *28*(11), 1375–1393. https://doi.org/10.1016/0198-0149(81)90039-X

Morin, P.-I., Lacour, T., Grondin, P.-L., Bruyant, F., Ferland, J., Forget, M.-H., Massicotte, P., Donaher, N., Campbell, D. A., Lavaud, J., & Babin, M. (2020). Response of the sea-ice diatom Fragilariopsis cylindrus to simulated polar night darkness and return to light. *Limnology and Oceanography*, *65*(5), 1041–1060. https://doi.org/10.1002/lno.11368

Mundy, C. J., Gosselin, M., Ehn, J. K., Belzile, C., Poulin, M., Alou, E., Roy, S., Hop, H., Lessard, S., Papakyriakou, T. N., Barber, D. G., & Stewart, J. (2011). Characteristics of two distinct high-light acclimated algal communities during advanced stages of sea ice melt. *Polar Biology*, *34*(12), 1869–1886. https://doi.org/10.1007/s00300-011-0998-x

Munekage, Y., Hashimoto, M., Miyake, C., Tomizawa, K. I., Endo, T., Tasaka, M., & Shikanai, T. (2004). Cyclic electron flow around photosystem I is essential for photosynthesis. *Nature*, *429*(6991), 579–582. https://doi.org/10.1038/nature02598

Olaizola, M., La Roche, J., Kolber, Z., & Falkowski, P. G. (1994). Non-photochemical fluorescence quenching and the diadinoxanthin cycle in a marine diatom. *Photosynthesis Research*, *41*, 357–370. https://doi.org/10.1007/BF00019413

Oziel, L., Massicotte, P., Randelhoff, A., Ferland, J., Vladoiu, A., Lacour, L., Galindo, V., Lambert-Girard, S., Dumont, D., Cuypers, Y., Bouruet-Aubertot, P., Mundy, C.-J., Ehn, J., Bécu, G., Marec, C., Forget, M.-H., Garcia, N., Coupel, P., Raimbault, P., … Babin, M. (2019). Environmental factors influencing the seasonal dynamics of spring algal blooms in and beneath sea ice in western Baffin Bay. *Elementa: Science of the Anthropocene*, *7*(1), 34. https://doi.org/10.1525/elementa.372

Padfield, D., O'Sullivan, H., & Pawar, S. (2021). rTPC and nls.Multstart: A new pipeline to fit thermal performance curves in R. *Methods in Ecology and Evolution*, *12*(6), 1138–1143. https://doi.org/10.1111/2041-210X.13585

Perrette, M., Yool, A., Quartly, G. D., & Popova, E. E. (2011). Near-ubiquity of ice-edge blooms in the Arctic. *Biogeosciences*, *8*(2), 515–524. https://doi.org/10.5194/bg-8-515-2011

Petrou, K., Doblin, M. A., & Ralph, P. J. (2011). Heterogeneity in the photoprotective capacity of three Antarctic diatoms during short-term changes in salinity and temperature. *Marine Biology*, *158*(5), 1029–1041. https://doi.org/10.1007/s00227-011-1628-4

Platt, T. G. C. L., Gallegos, C. L., & Glen Harrison, W. (1980). Photoinhibition of photosynthesis in natural assemblages of marine phytoplankton. *Journal of Marine Research*, *38*, 687–701. Retrieved from https://pdfs.semanticscholar.org/9cc6/f2193c174000

Poulin, M., Daugbjerg, N., Gradinger, R., Ilyash, L., Ratkova, T., & von Quillfeldt, C. (2011). The pan-Arctic biodiversity of marine pelagic and sea-ice unicellular eukaryotes: A first-attempt assessment. *Marine Biodiversity*, *41*(1), 13–28. https://doi.org/10.1007/s12526-010-0058-8

Randelhoff, A., Lacour, L., Marec, C., Leymarie, E., Lagunas, J., Xing, X., Darnis, G., Penkerc'h, C., Sampei, M., Fortier, L., D'Ortenzio, F., Claustre, H., & Babin, M. (2020). Arctic mid-winter phytoplankton growth revealed by autonomous profilers. *Science Advances*, *6*(39), eabc2678. https://doi.org/10.1126/sciadv.abc2678

Randelhoff, A., Oziel, L., Massicotte, P., Bécu, G., Galí, M., Léo, L., Dumont, D., Vladoiu, A., Marec, C., Bruyant, F., Houssais, M.-N., Tremblay, J.-É., Deslongchamps, G., & Babin, M. (2019). The evolution of light and vertical mixing across a phytoplankton ice-edge bloom. *Elementa: Science of the Anthropocene*, *7*(1), 20. https://doi.org/10.1525/elementa.357

Ras, J., Claustre, H., & Uitz, J. (2008). Spatial variability of phytoplankton pigment distributions in the subtropical South Pacific Ocean: Comparison between in situ and predicted data. *Biogeosciences*, *5*(2), 353–369. https://doi.org/10.5194/bg-5-353-2008

Sakshaug, E., Johnsen, G., Andresen, K., & Vernet, M. (1991). Modeling of light-dependent algal photosynthesis and growth: Experiments with the Barents Sea diatoms *Thalassiosira nordenskioldii* and *Chaetoceros furcellatus*. *Deep Sea Research Part A, Oceanographic Research Papers*, *38*(4), 415–430. https://doi.org/10.1016/0198-0149(91)90044-G

Sathyendranath, S., Stuart, V., Nair, A., Oka, K., Nakane, T., Bouman, H., Forget, M.-H., Maass, H., & Platt, T. (2009). Carbon-to-chlorophyll ratio and growth rate of phytoplankton in the sea. *Marine Ecology Progress Series*, *383*, 73–84. https://doi.org/10.3354/meps07998

Schuback, N., Hoppe, C. J. M., Tremblay, J. É., Maldonado, M. T., & Tortell, P. D. (2017). Primary productivity and the coupling of photosynthetic electron transport and carbon fixation in the Arctic Ocean. *Limnology and Oceanography*, *62*(3), 898–921. https://doi.org/10.1002/lno.10475

Shatwell, T., Köhler, J., & Nicklisch, A. (2013). Temperature and photoperiod interactions with silicon-limited growth and competition of two diatoms. *Journal of Plankton Research*, *35*(5), 957–971. https://doi.org/10.1093/plankt/fbt058

Sigmond, M., Fyfe, J. C., & Swart, N. C. (2018). Ice-free Arctic projections under the Paris agreement. *Nature Climate Change*, *8*(5), 404–408. https://doi.org/10.1038/s41558-018-0124-y

Smetacek, V., Assmy, P., & Henjes, J. (2004). The role of grazing in structuring Southern Ocean pelagic ecosystems and biogeochemical cycles. *Antarctic Science*, *16*(4), 541–558. https://doi.org/10.1017/S0954102004002317

Sommer, U., Adrian, R., De Senerpont Domis, L., Elser, J. J., Gaedke, U., Ibelings, B., Jeppesen, E., Lürling, M., Molinero, J. C., Mooij, W. M., van Donk, E., & Winder, M. (2012). Beyond the plankton ecology group (PEG) model: Mechanisms driving plankton succession. *Annual Review of Ecology, Evolution, and Systematics*, *43*(1), 429–448. https://doi.org/10.1146/annurev-ecolsys-110411-160251

Strzepek, R. F., Boyd, P. W., & Sunda, W. G. (2019). Photosynthetic adaptation to low iron, light, and temperature in Southern Ocean phytoplankton. *Proceedings of the National Academy of Sciences of the United States of America*, *116*(10), 4388–4393. https://doi.org/10.1073/pnas.1810886116

Thomas, D. N., & Dieckmann, G. S. (2002). Antarctic sea ice–a habitat for extremophiles. *Science*, *295*(5555), 641–644. https://doi.org/10.1126/science.1063391

von Quillfeldt, C. H. (2000). Common diatom species in arctic spring blooms: Their distribution and abundance. *Botanica Marina*, *43*(6), 499–516. https://doi.org/10.1515/bot.2000.050

Wagner, H., Jakob, T., Lavaud, J., & Wilhelm, C. (2016). Photosystem II cycle activity and alternative electron transport in the diatom *Phaeodactylum tricornutum* under dynamic light conditions and nitrogen limitation. *Photosynthesis Research*, *128*(2), 151–161. https://doi.org/10.1007/s11120-015-0209-7

Wood, A., Everroad, R., & Wingard, L. (2005). Measuring growth rates in microalgal cultures. Algal culturing techniques. In R. Anderson (Ed.), *Algal culturing techniques* (pp. 269–285). Elsevier Academic Press.

Young, J. N., Goldman, J. A. L., Kranz, S. A., Tortell, P. D., & Morel, F. M. M. (2015). Slow carboxylation of rubisco constrains the rate of carbon fixation during Antarctic phytoplankton blooms. *New Phytologist*, *205*(1), 172–181. https://doi.org/10.1111/nph.13021

Zhu, Y., Suggett, D. J., Liu, C., He, J., Lin, L., Le, F., Ishizaka, J., Goes, J., & Hao, Q. (2019). Primary productivity dynamics in the summer arctic ocean confirms broad regulation of the electron requirement for carbon fixation by light-phytoplankton community interaction. *Frontiers in Marine Science*, *6*, 275. https://doi.org/10.3389/fmars.2019.00275

SUPPORTING INFORMATION

Additional supporting information may be found in the online version of the article at the publisher's website.

How to cite this article: Croteau, D., Lacour, T., Schiffrine, N., Morin, P-I, Forget, M-H, Bruyant, F., Ferland, J., Lafond, A., Campbell, D. A., Tremblay, J-É, Babin, M. & Lavaud, J. (2022). Shifts in growth light optima among diatom species support their succession during the spring bloom in the Arctic. *Journal of Ecology*, *00*, 1–20. https://doi.org/10.1111/1365-2745.13874